Cellular & Molecular Biology Letters

https://doi.org/10.1186/s11658-026-00983-z

Article in Press

Cannabidiol alleviates traumatic brain injury-induced neuronal damage and cognitive deficits by inhibiting ferroptosis via the TRPV1/MCU/PI3K/Akt pathway

Received: 3 August 2025

Accepted: 11 June 2026

Published online: 27 June 2026

Cite this article as: Xu Y., Li X., Gu Z. *et al.* Cannabidiol alleviates traumatic brain injury-induced neuronal damage and cognitive deficits by inhibiting ferroptosis via the TRPV1/MCU/PI3K/Akt pathway. *Cell Mol Biol Lett* (2026). https://doi.org/10.1186/s11658-026-00983-z

Yejia Xu, Xiong Li, Zhiya Gu, Xuehua Chen, Yang Zhao, Bowen Jia, Yumeng Wu, Rui Wan, Qianqian Li, Tao Wang & Chengliang Luo

Cannabidiol alleviates traumatic brain injury–induced neuronal damage and cognitive deficits by inhibiting ferroptosis via the TRPV1/MCU/PI3K/Akt pathway

Yejia Xu [1, 2†], Xiong Li [1†], Zhiya Gu [2†], Xuehua Chen [1], Yang Zhao [1], Bowen Jia [2], Yumeng Wu [1], Rui Wan [1], Qianqian Li [1*], Tao Wang [2*], Chengliang Luo [1*]

[1] Department of Forensic Medicine, School of Forensic Medicine, National Health Commission Key Laboratory of Drug Addiction Medicine, Kunming Medical University, Kunming 650500, China.

[2] Jiangsu Key Laboratory of Drug Discovery and Translational Research for Brain Diseases, School of Basic Medical Sciences, Soochow University, Suzhou, Jiangsu 215123, China.

*Correspondence: bzliqian@126.com; taowang@suda.edu.cn; luochengliang@kmmu.edu.cn

[†]These authors contributed equally to this work.

Abstract

Background: Traumatic brain injury (TBI) is a common surgical traumatic condition that poses a significant threat to human health and working capacity. However, effective treatments to improve its prognosis remain limited. Cannabidiol (CBD), a naturally occurring compound extracted

from the cannabis plant, exhibits multiple pharmacological effects through diverse molecular targets. To date, the role and underlying molecular mechanisms of CBD in the context of TBI have not been fully elucidated. In this study, we investigated the specific effects of CBD following TBI and explored its underlying mechanisms.

Methods: An *in vitro* ferroptosis model was established using HT-22 cells, and an *in vivo* TBI model was established in mice. Techniques such as Western blotting, immunofluorescence staining, and behavioral analysis were employed to evaluate the effects of CBD on ferroptosis, pathological changes, and neurological function after TBI, as well as to explore the associated molecular mechanisms.

Results: CBD significantly alleviated ferroptosis, neuronal injury, and cognitive dysfunction following TBI *in vitro and in vivo*. Further investigation revealed that CBD mitigated mitochondrial dysfunction by reducing Ca^{2+} overload via the TRPV1/MCU signaling pathway. Moreover, utilizing methodologies such as recombinant adeno-associated virus (rAAV) injection and transcriptome analysis, mitochondrial calcium uniporter (MCU) was identified as a core regulator of ferroptosis in neurons following TBI. Neuronal MCU knockdown attenuated the progression of ferroptosis and improved neurological outcomes after TBI. Finally, integrated findings confirmed that CBD inhibit ferroptosis after

TBI through the TRPV1/MCU/PI3K/Akt signaling pathway.

Conclusion: CBD inhibits ferroptosis, at least in part, via the TRPV1/MCU/PI3K/Akt signaling pathway, thereby alleviating TBI-induced neuronal damage and cognitive deficits. In addition, these findings indicate that CBD exhibits a potent anti-ferroptotic effect and may serve as a promising therapeutic agent for TBI.

Keywords: Cannabidiol, Traumatic brain injury, Ferroptosis, Mitochondrial calcium uniporter, Cognitive deficits, TRPV1/MCU/PI3K/Akt signaling pathway

Introduction

Traumatic brain injury (TBI), caused by direct or indirect mechanical forces, remains one of the leading causes of death and disability globally, both historically and prospectively [1]. Recent epidemiological data indicate that the severity of TBI is closely associated with increased unemployment and decreased personal income, thereby imposing a significant socioeconomic burden [2]. While the primary injury causes immediate and direct neuronal damage, it is the secondary injury that significantly exacerbates disease progression. This secondary phase involves sustained axonal damage and is driven by a complex cascade of

biochemical events, including metabolic dysfunction, excitotoxicity, neuroinflammation, and oxidative stress [3]. Current therapeutic interventions targeting TBI-induced cognitive, language, and behavioral impairments are limited, focusing primarily on symptomatic pharmacological management and physical rehabilitation [4, 5]. Therefore, identifying effective strategies to mitigate secondary injury has become a central goal in post-TBI recovery research.

The endocannabinoid system has emerged as a promising therapeutic target for TBI, as cannabinoids interact with neurons, microglia, and astrocytes to exert anti-inflammatory and neuroprotective effects [6]. The synthetic cannabinoid analogue dexanabinol (HU-211) was one of the first cannabinoids to undergo extensive clinical evaluation for TBI. Preclinical studies demonstrated its neuroprotective effects through NMDA receptor antagonism and inhibition of TNF-α production [7-9]. Following encouraging Phase II results showing reduced intracranial pressure and improved outcomes in patients with severe head injury [10], a large Phase III randomized, placebo-controlled trial involving 861 patients with severe TBI was conducted. Unfortunately, dexanabinol failed to demonstrate a significant improvement in neurological outcomes at six months post-injury, highlighting the challenges of translating cannabinoid-based therapies from preclinical models to clinical practice [11].

Cannabidiol (CBD), a non-intoxicating phytochemical derived from *Cannabis sativa*, has gained increasing attention as a potential therapeutic agent [12]. Unlike tetrahydrocannabinol (THC), CBD does not directly activate cannabinoid receptors CB1 or CB2; rather, recent studies suggest that it may act as an antagonist or, more accurately, a negative allosteric modulator of these receptors. This distinctive mechanism of action contributes to its lower risk of addiction and a favorable safety profile [13]. Due to its broad interaction with multiple cellular targets and signaling pathways, CBD exerts diverse biological effects, including the modulation of neuroinflammation and oxidative stress [14, 15]. A growing body of evidence has investigated the neuroprotective potential of CBD following TBI. TBI-induced damage cascades and the neuroprotective mechanisms of CBD—including its effects on neurotransmitter systems, the blood-brain barrier, oxidative stress, and the inflammatory response—have been systematically described [16]. Preclinical evidence suggests that CBD holds great promise as a much-needed improvement in the clinical treatment of TBI, with upcoming clinical trials sponsored by major professional sport leagues representing the first attempts to test its efficacy in head injury treatment protocols [16]. Major and minor phytocannabinoids, terpenes, synthetic cannabinoids, and endogenous cannabinoids have also been comprehensively appraised in preclinical TBI

models and clinical TBI populations. In the context of mild TBI and concussion, CBD has been proposed to enhance neuroprotection by reducing inflammation, regulating cerebral blood flow, enhancing neurogenesis, and protecting the brain against reactive oxygen species [17]. Despite these promising preclinical findings, recent studies have begun to explore the potential of CBD to improve cognitive outcomes following TBI; however, the mechanisms by which CBD mitigates neuronal damage during the secondary phase of TBI remain poorly understood.

Ferroptosis, a newly identified form of regulated cell death first described in 2012, is characterized by intracellular iron accumulation, lipid peroxidation, and an imbalance in antioxidant defenses [19]. Evidence indicates that ferroptosis is involved at various stages after TBI, contributing to neuronal degeneration [20]. Importantly, elevated levels of ferroptosis-related markers, such as malondialdehyde (MDA) and 4-hydroxynonenal (4-hne), have been positively correlated with the severity of neurological deficits and poorer functional outcomes in TBI models [21]. Notably, the crosstalk of cannabinoids and ferroptosis has recently gained attention. A study by Liang et al. (2024) dismonstrated that cannabinol (CBN), another non-psychoactive cannabinoid, functions as a unique inhibitor of ferroptosis by targeting mitochondria and modulating their function in neuronal cells [22]. The authors further developed novel CBN

analogs that prevented mitochondrial dysfunction and demonstrated in vivo efficacy in a fly model of mild TBI [22]. These findings further support the notion that cannabinoid-mediated ferroptosis inhibition represents a promising therapeutic direction for TBI. Given the strong interplay between ferroptosis, neuroinflammation, and oxidative stress, the hypothesis that CBD may inhibit ferroptosis via specific signaling pathways represents a novel and promising research direction [23, 24].

Transient receptor potential vanilloid 1 (TRPV1) is an ion channel predominantly expressed in neurons [25]. CBD has been shown to activate and subsequently desensitize TRPV1, leading to altered membrane potentials and intracellular ion concentrations [26]. TRPV1-mediated calcium influx has been implicated in the activation of reactive oxygen species (ROS) and mitochondrial dysfunction [27]. The mitochondrial calcium uniporter (MCU), located on the inner mitochondrial membrane, regulates calcium homeostasis between the cytoplasm and mitochondria [28]. Altered MCU activity influences cellular oxidative stress, and recent findings suggest that downregulation of MCU expression may suppress neuronal ferroptosis by limiting mitochondrial ROS production [29]. The phosphoinositide 3-kinase/protein kinase B (PI3K/Akt) pathway, a crucial regulator of cell growth and survival, also appears to act as a ferroptosis inhibitor in TBI models [30]. Notably, calcium signaling has been shown

to modulate this pathway and alleviate injury in various tissues [31].

Based on a murine TBI model and a ferroptosis model using HT-22 neuronal cells, this study integrates transcriptomic data to investigate the role of CBD in inhibiting neuronal ferroptosis following TBI. Specifically, we examine how CBD regulates intracellular calcium homeostasis via the TRPV1/MCU/PI3K/Akt axis to mitigate ferroptotic cell death. These findings are intended to establish a mechanistic framework for the potential therapeutic use of CBD in improving cognitive dysfunction associated with TBI.

Materials and methods

Animal

All animal procedures were reviewed and approved by the Ethics Committees of Kunming Medical University and Soochow University (China). Adult male C57BL/6J mice (20–25 g) were obtained from the Animal Center of the Chinese Academy of Sciences (Shanghai, China). All mice were housed under standardized conditions: a 12-hour light/dark cycle, a controlled temperature of 25 °C, a relative humidity of 50%, and ad libitum access to food and water.

Mouse TBI model

Adult male C57BL/6J mice (20–25 g) were randomly assigned to sham or

intervention groups. TBI was induced in the intervention group using a standardized controlled cortical impact (CCI) model to mimic clinical TBI. Briefly, mice were anesthetized via intraperitoneal injection of sodium pentobarbital (10 mg/kg) and placed in a prone position using a stereotaxic frame (RWD Life Science Co., Shenzhen, China). Following a midline scalp incision, the skull was exposed, and a 4 mm craniotomy was performed on the left side between the bregma and lambda, adjacent to the sagittal suture, with the dura mater left intact. A pneumatic impactor (AmScien Instruments, USA) was applied perpendicularly to the exposed cortex using fixed parameters: impact pressure of 100 kPa, depth of 1 mm, and dwell time of 80 ms. After the procedure, the scalp was sutured immediately, and mice were monitored until full recovery. Sham-operated mice underwent all procedures except for the cortical impact. At designated time points post-injury, mice were sacrificed, and cortical tissue was collected from the ipsilateral (injured) hemisphere for further biological analyses.

Drug preparation

CBD was purchased from Abmole (Cat. No. 13956-29-1). It was initially dissolved in Tween-80 (final concentration: 1%) and subsequently diluted with normal saline for administration. Liproxstatin-1 (Lip-1), a ferroptosis inhibitor, was obtained from GLPBIO (Cat. No. GC15681). Lip-1 was

dissolved in DMSO (final concentration: 0.5%) and then diluted with normal saline. Capsazepine, a synthetic TRPV1 receptor antagonist, was purchased from GLPBIO (Cat. No. GC17918). It was dissolved in DMSO (final concentration 2%) and then diluted with corn oil. Ru360, a selective inhibitor of the MCU, was obtained from Sigma-Aldrich (Cat. No. 557440). It was dissolved in double-distilled water and then diluted with physiological saline. Gdc-0941, a PI3K inhibitor, was purchased from GLPBIO (Cat. No. GC10816). The powder was dissolved in DMSO (final concentration 2%) and then diluted with PEG300 (final concentration 30%), Tween-80 (final concentration 5%), and double-distilled water.

For *in vivo* experiments, mice in the TBI+CBD group received an intraperitoneal injection of CBD at a dose of 10 mg/kg, administered 30 min post-TBI induction [32]. Mice in the TBI+Lip-1 group were administered Lip-1 intraperitoneally at a dose of 10 mg/kg, 1 h after TBI [30]. Mice in the Sham + Capsazepine and TBI + Capsazepine groups received an intraperitoneal injection of capsazepine at a dose of 5 mg/kg at 30 min after the sham operation or TBI induction. Mice in the TBI + Ru360 group received an intraperitoneal injection of Ru360 at a dose of 120 μg/kg at 30 min after TBI. In the TBI + CBD + gdc-0941 group, gdc-0941 (5 mg/kg, i.p.) was administered at 15 minutes after TBI, followed by CBD (10 mg/kg, i.p.) at 30 min post-TBI.

RSL3, a ferroptosis inducer, was purchased from MedChemExpress (Cat. No. HY-100218A). Based on our preliminary studies, HT-22 cells were treated with RSL3 at a concentration of 0.2 μM [33]. CBD and Lip-1 were used to treat HT-22 cells at concentrations of 0.3 μM and 0.2 μM, respectively [34, 35].

Experimental design

Part 1: To investigate the effects of CBD on cognitive function following TBI and its potential association with ferroptosis, mice were randomly assigned (n = 6 per group) to the following four groups: Sham, TBI+Vehicle, TBI+CBD, and TBI+Lip-1. All mice received intraperitoneal injections of the respective treatments or vehicle (normal saline) 30 min after TBI induction. Brain samples were subsequently analyzed using Western blotting, Perls' Prussian blue staining, Nissl staining, Fluoro-Jade B (FJB) staining, immunofluorescence, and behavioral analysis.

Part 2: To evaluate the anti-ferroptotic and neuroprotective effects of CBD at the cellular level, HT-22 cells were divided into four groups: control, RSL3, RSL3+CBD, and RSL3+Lip-1. Following treatment, the cells were subjected to lipid ROS assays, cytoplasmic and mitochondrial ferrous ion (Fe^{2+}) detection, cytoplasmic and mitochondrial Ca^{2+} measurements, and JC-1 staining for mitochondrial membrane potential

assessment.

Part 3: To assess the regulatory role of recombinant adeno-associated virus (rAAV)-mediated knockdown of the MCU *in vivo*, mice were randomly divided into four groups (n = 6 per group): control-sham, sh(MCU)-sham, control-TBI, and sh(MCU)-TBI. After rAAV transfection, mice were allowed to recover for 21 days before TBI modeling. Cortical tissue from the injured hemisphere was collected 24 h post-injury. Western blotting, Perls' staining, Nissl staining, FJB staining, immunofluorescence, and behavioral tests were conducted.

Part 4: To further verify the mechanistic involvement of MCU in ferroptosis, MCU was overexpressed via rAAV in the following groups (n = 6 per group): control-sham, OE(MCU)-sham, control-TBI, and OE(MCU)-TBI. Western blotting was used to assess the expression levels of ferroptosis-related proteins in cortical tissues.

Part 5: To elucidate the role of MCU in ferroptosis and neural function *in vitro*, HT-22 cells were divided into four groups: control, si-MCU, RSL3, and RSL3+si-MCU. The experimental analyses included cytoplasmic and mitochondrial Fe^{2+} detection, lipid ROS assays, and mitochondrial Ca^{2+} measurements.

Part 6: To explore the molecular interaction between TRPV1 and MCU,

and to clarify the role of TRPV1 in CBD-mediated ferroptosis inhibition, HT-22 cells were divided into four groups: control, si-TRPV1, RSL3, and RSL3+si-TRPV1. Western blotting analysis was performed to examine the expression of relevant signaling proteins.

Part 7: To further demonstrate the role of TRPV1 in MCU phosphorylation, mice were randomly divided into the following four groups (n = 6 per group): Sham+Vehicle, TBI+Vehicle, Sham+Capsazepine, and TBI+Capsazepine. All mice received an intraperitoneal injection of capsazepine or normal saline 30 min after TBI or sham operation. Brain samples were primarily used for Western blotting to compare the pMCU/MCU ratio.

Part 8: To investigate how MCU regulation affects downstream signaling pathways, mice were randomly assigned to two groups (n = 6 per group): TBI+Vehicle and TBI+Ru360. Ru360 or normal saline was administered via intraperitoneal injection 30 min after TBI. Cerebral cortex samples were then collected and analyzed by Western blotting to evaluate changes in the PI3K/Akt signaling pathway and the extent of ferroptosis.

Part 9: To further explore the broader link between the PI3K pathway and the neuroprotective effects of CBD, mice were randomly assigned to two groups for a rescue experiment (n = 6 per group): TBI+CBD and TBI+CBD+gdc-0941. All mice received an intraperitoneal injection of

either gdc-0941 or normal saline at 15 min post-TBI, followed by an intraperitoneal injection of CBD at 30 min post-TBI. After tissue collection, the cerebral cortex was analyzed by western blotting to assess changes in the expression of proteins associated with ferroptosis or neuroprotection.

Recombinant adeno-associated virus injection

Briefly, mice were anesthetized and placed in a stereotaxic apparatus (RWD Life Science Co., Shenzhen, China) for intracerebral injection. A microsyringe was used to deliver 1 μL of the following recombinant adeno-associated viruses (rAAV) into the cerebral cortex at the following coordinates: anteroposterior (AP): −1.5 mm, mediolateral (ML): 2.0 mm, dorsoventral (DV): −1.0 mm. The viral constructs included rAAV-hSyn-MCU-EGFP-WPRE -hGH polyA, rAAV-hSyn-EGFP-WPRE-hGH polyA, rAAV-hSyn-EGFP-5'miR- 30a-shRNA (MCU)-3' -miR30a -WPRE, and rAAV-hSyn-EGFP -5'miR-30a-shRNA(scramble) -3' -miR30a-WPRE (Supporting Material: Table S1). The injection was performed at a rate of 0.2 μL/min over a duration of 5 min. Upon completion, the needle was slowly withdrawn, and the scalp was sutured. Mice were then allowed to recover under standard conditions.

RNA extraction and transcriptome analysis of cerebral cortex tissues

Total RNA was extracted from cerebral cortex tissues surrounding the lesion sites in four experimental groups: control-TBI, sh-TBI, TBI+vehicle,

and TBI+CBD (n = 3 per group). Tissue samples were collected 24 h after TBI induction, immediately frozen in liquid nitrogen, and sent to GENEWIZ Biotechnology Co., Ltd. (Suzhou, China) for RNA purification, reverse transcription, library preparation, and sequencing.

RNA was extracted using l™ Reagent (equivalent to Trizol Reagent). For transcriptome analysis, mRNA was enriched from total RNA using oligo(dT) magnetic beads, and sequencing libraries were constructed using the VAHTS® Universal V8 RNA-Seq Library Prep Kit for Illumina. Sequencing was performed on the Illumina® NovaSeq X Plus platform.

Differential expression analysis between groups was conducted using the DESeq2 package. Genes with a p-value < 0.05 and $|\log_2 \text{fold change}| > \log_2 1.5$ were considered significantly differentially expressed. Functional enrichment of differentially expressed genes (DEGs) was performed using the clusterProfiler package for Gene Ontology (GO) and Kyoto Encyclopedia of Genes and Genomes (KEGG) analyses (pvalue < 0.05). In addition, Gene Set Enrichment Analysis (GSEA) was employed to assess continuous expression trends, with significance set at an FDR padj < 0.25.

Western blotting

Western blotting was performed following our previously established protocol [36]. Cerebral cortex tissues were lysed in RIPA lysis buffer

(Beyotime, Jiangsu, China) supplemented with phenylmethanesulfonyl fluoride (PMSF; Beyotime, Jiangsu, China) at a 100:1 volume ratio. The lysates were incubated on ice until complete tissue lysis and then centrifuged at 12,000 rpm for 25 min at 4°C. The protein concentration of the supernatant was quantified using a NanoDrop 2000C spectrophotometer (Thermo Scientific, USA).

Equal amounts of protein (25 μg) were separated on 10% or 12% SDS-PAGE gels (Vazyme, China) and transferred onto polyvinylidene fluoride (PVDF) membranes (Millipore, Boston, MA, USA). Membranes were blocked for 20 min using Protein-Free Rapid Blocking Buffer (Yaenzyme, Shanghai, China), followed by overnight incubation at 4°C with the appropriate primary antibodies. After three 5-min washes with TBST, membranes were incubated with HRP-conjugated secondary antibodies at room temperature for 2 h.

Protein bands were visualized using an enhanced chemiluminescence (ECL) system (ChemiScope, Shanghai, China) and quantified using ImageJ software (NIH). Protein expression levels were normalized to β-tubulin. Detailed information on the primary and secondary antibodies used is provided in Supporting Material: Table S2.

Immunofluorescence staining

Mouse brains were harvested, rapidly frozen, and sectioned into 10 μm-

thick slices using a cryostat. The frozen sections were first equilibrated to room temperature, then fixed with 4% paraformaldehyde for 30 min. After fixation, sections were washed with phosphate-buffered saline (PBS) for 5 min, repeated three times.

Blocking was performed by incubating the sections with 5% bovine serum albumin (BSA) in PBS for 2 h at room temperature. Subsequently, the sections were incubated overnight at 4°C with primary antibodies. After washing with PBS (3 × 5 min), the sections were incubated with fluorescently labeled secondary antibodies for 2 h at room temperature.

DAPI (Beyotime Biotechnology, China) was diluted in PBS at a ratio of 1:10,000 and applied to the sections for 1 min to stain cell nuclei. Fluorescence images were captured using a Nikon TE300 fluorescence microscope (Nikon, Japan), and fluorescence intensity was quantified using ImageJ software (NIH).

Enhanced Perls' Pussian blue staining

Frozen brain sections were air-dried at room temperature for 5 min and then washed with phosphate-buffered saline with Tween-20 (PBST) for 5 min. The sections were briefly immersed in 95% ethanol for 15 seconds, followed by incubation with Perls' staining solution (Solarbio, Cat. No. G1424) for 40 min at room temperature. After another PBST wash (5 min), 0.3% hydrogen peroxide diluted in methanol was applied to the sections

for 15 min to quench endogenous peroxidase activity.

Following a final PBST wash, brain sections were incubated with 3,3'-diaminobenzidine (DAB) for 15 min to visualize iron deposition. Nuclei were counterstained with hematoxylin, rinsed with tap water for 5 min, and dehydrated through an ethanol gradient. Images were captured using a Nikon TE300 microscope (Nikon, Japan).

Nissl staining

After equilibrating to room temperature, brain sections were sequentially immersed in 75% ethanol for 15 min and 90% ethanol for 25 min. Nissl staining solution (Beyotime, China) was then applied to the sections and incubated for 5 min. Following staining, the sections were rinsed with distilled water at 25 °C for 5 min. Nissl-positive neurons were visualized and imaged using a Nikon TE300 microscope (Nikon, Japan).

Fluoro-Jade B (FJB) staining

Brain sections were dried at 50°C for 30 min, followed by fixation with 4% paraformaldehyde for 1 h at room temperature. The sections were then immersed sequentially in 1% sodium hydroxide and 80% ethanol for 5 min each. Afterward, they were rinsed with 80% ethanol and distilled water for 2 min each.

Next, 0.06% potassium permanganate solution was applied dropwise to

the sections and incubated for 10 min, followed by washing with distilled water. Subsequently, 0.0004% Fluoro-Jade B solution was added dropwise, and the sections were incubated for 30 min in the dark. Fluorescent images were captured using a Nikon TE300 fluorescence microscope (Nikon, Japan).

Behavioral analysis

Motor function was assessed using the wire-grip test from days 1 to 5 following CCI injury. Mice were placed on an inverted wire grid elevated 45 cm above the ground, and performance was evaluated using a standardized five-point scale. Each mouse underwent two trials, and the average score was recorded. All behavioral assessments were performed by an experimenter blinded to the group allocation. Sample size (n = 8 per group) was determined based on previous experimental experience to ensure adequate statistical power.

On day 6 post-CCI, anxiety-like behavior was evaluated using the open field test. Mice were placed in a 30 cm × 30 cm open field arena, and their locomotor activity and exploratory behavior were recorded using an automated behavioral tracking system (JLBehv-OFG-4, Shanghai Jilang Software Technology Co., Ltd., Shanghai, China). The experimenter conducting the test and analyzing the data was blinded to treatment conditions.

Cognitive function was assessed using the Morris Water Maze (MWM) test conducted between days 9 and 13 post-CCI. Prior to CCI induction, all mice underwent 7 days of training to locate a hidden platform. During the testing period, a video tracking system was used to monitor swimming trajectories, escape latency, and platform crossing frequency, and the percentage of time spent in the target quadrant. Behavioral scoring and analysis were performed blind to group assignment.

On day 15 post-CCI, depressive-like behavior was evaluated using the tail suspension test. Mice were suspended by the tail, and the duration of immobility was recorded as an index of behavioral despair. The same blinding procedure was applied.

Lesion volume assessment

After completion of behavioral testing, the mice were sacrificed and their brains were sectioned using a cryostat to obtain frozen coronal sections. The sections were stained with hematoxylin at room temperature for 10 min, followed by rinsing with double-distilled water for 5 min. Lesion volume was assessed via microscopic imaging. The relative volume of brain tissue loss was calculated using the following formula:(Area of healthy hemisphere − Area of injured hemisphere) / Area of healthy hemisphere × 2.

Cell culture and transfection

HT-22 cells (mlsw-3040, mlBio, Shanghai, China) were cultured in Dulbecco's Modified Eagle Medium (DMEM; Gibco, USA) supplemented with 10% fetal bovine serum (FBS; Gibco), 1% penicillin-streptomycin, and maintained in a humidified incubator at 37°C with 5% CO_2.

For gene silencing, HT-22 cells were transfected with siRNA targeting MCU or TRPV1. Briefly, siRNA was diluted with RNase-free water to prepare a 20 μM stock solution. Lipofectamine 2000 (Beyotime, China) and siRNA were each diluted separately with Opti-MEM (Gibco) and incubated at room temperature for 5 min. Equal volumes of diluted Lipofectamine and siRNA were mixed and incubated for 20 min to form complexes. A total of 500 μL of the mixture was added to 1.5 mL of culture medium per well in a six-well plate. The final siRNA concentration was 50 nM.

Lipid ROS assay

Lipid peroxidation was assessed using BODIPY^{TM} 581/591 C11 dye (GLPBIO, USA). After intervention, cells were washed with Hank's Balanced Salt Solution (HBSS) and incubated with 2 μM BODIPY C11 working solution (200 μL per coverslip) at 37 °C for 30 min. After three washes with HBSS, cells were imaged using a fluorescence microscope (Nikon TE300, Japan).

Fe^{2+} detection in cytoplasm and mitochondria

Intracellular and mitochondrial Fe^{2+} levels were measured using FerroOrange and Mito-FerroGreen dyes (Dojindo, Japan), respectively. Following intervention, cells were washed with HBSS and then incubated with 1 μM (FerroOrange) or 5 μM (Mito-FerroGreen) working solution (200 μL per coverslip) at 37 °C for 30 min. After three HBSS washes, fluorescence images were acquired with a Nikon TE300 microscope.

Ca^{2+} detection in cytoplasm and mitochondria

Cytoplasmic and mitochondrial Ca^{2+} levels were measured using Fluo-4 AM (GC30231, GLPBIO) and Rhod-2 AM (GC30506, GLPBIO) fluorescent probes, respectively. Stock solutions (1 mM) were prepared in DMSO and diluted with PBS containing 0.02% Pluronic F-127 (GLPBIO) to make 1 μM working solutions. Cells were incubated with 200 μL of the working solution per coverslip at 37 °C for 30 min. After three washes with HBSS, images were captured under a fluorescence microscope (Nikon TE300, Japan).

Mitochondrial membrane potential (Δψm) assay

Mitochondrial membrane potential was assessed using the JC-1 assay kit (Beyotime, China). The JC-1 working solution was prepared according to the manufacturer's instructions and mixed with complete medium in a 1:1 ratio. Cells were incubated with the mixture at 37°C for 1 h, washed with

HBSS, and imaged using a fluorescence microscope (Nikon TE300, Japan).

Assay for GSH/GSSG

Briefly, tissue samples from the ipsilateral cortex were weighed and then homogenized in ice-chilled PBS. The resulting homogenates were centrifuged at 10,000–12,000 × g for 10 min at 4°C, and the clear supernatant was carefully collected for subsequent analysis. The levels of reduced glutathione (GSH) in the cortical samples were measured using a commercially available GSH and GSSG Assay Kit (catalog #S0053, Beyotime Biotechnology, Shanghai, China), following the manufacturer's recommended protocol. The absorbance of each reaction mixture was determined at 593 nm using a colorimetric microplate reader (Thermo Scientific Multiskan FC). The GSH content was normalized to the tissue wet weight and expressed as micromoles per gram (μmol/g). The concentration of GSH in the test samples was calculated using the formula: Total Glutathione − GSSG × 2.

Statistical analysis

All data are presented as mean ± standard deviation (SD). Statistical analyses were performed using GraphPad Prism 9.2 software (GraphPad Software Inc., San Diego, USA). Comparisons between two groups were conducted using the Student’s t-test, while comparisons among multiple groups were performed using one-way ANOVA followed by Tukey’s post

hoc test. All statistical tests were two-tailed, and a *p*-value < 0.05 was considered statistically significant.

Results

CBD alleviates neuronal pathological changes and behavioral deficits induced by TBI

To investigate the effect of CBD on TBI-induced alterations in neural structure and function, we first performed Fluoro-Jade B and Nissl staining on brain sections to assess neuronal damage. In the TBI+vehicle group, a significant increase in positively stained degenerating or dying neurons was observed in the perilesional cortex compared to the sham group (Fig. 1A, D). In contrast, brain sections from the TBI+CBD group showed a marked reduction in neuronal degeneration, resembling the neuroprotective effects observed in the TBI+Lip-1 group (Fig. 1A, D). Consistent with these findings, Nissl staining performed one day post-TBI revealed nuclear condensation and cytoplasmic shrinkage in the TBI+vehicle group, whereas both CBD and Lip-1 treatments attenuated Nissl body loss and preserved neuronal morphology (Fig. 1B).

We then assessed the expression of synaptic plasticity-related proteins by Western blotting. Brain-Derived Neurotrophic Factor (BDNF), a neurotrophin family member, is known to enhance neuronal synaptic plasticity [37]. One day after TBI, BDNF expression was significantly

reduced in the cortex, whereas treatment with CBD or Lip-1 mitigated this decrease (Fig. 1C, E, F). In addition, postsynaptic density protein 95 (psd-95), a major scaffolding protein in the postsynaptic membrane closely associated with synaptic remodeling [38], was markedly increased in the TBI+vehicle group compared to the sham group. Both CBD and Lip-1 treatments partially reversed this pathological elevation (Fig. 1C, E, F).

To evaluate the functional consequences of these structural alterations, we conducted behavioral tests, including the wire grip test, open field test, Morris water maze, and tail suspension test (Fig. 2A). In the wire grip test, the motor performance scores of the TBI+CBD and TBI+Lip-1 groups fell between those of the sham and TBI+vehicle groups. By day 5, all four groups had largely recovered their grip strength (Fig. 2B). On day 6 post-TBI, the open field test revealed that the central activity distance in the sham, TBI+CBD, and TBI+Lip-1 groups was significantly greater than that in the TBI+vehicle group, indicating that both CBD and Lip-1 effectively alleviated the anxiety-like behaviors induced by TBI (Fig. 2C, D). Morris water maze results further demonstrated that both CBD and Lip-1 reversed TBI-induced memory impairments, as evidenced by improved escape latency and swimming trajectories (Fig. 2F, G). On the final day of testing, the number of platform crossings within 90 seconds was significantly increased in the CBD- and Lip-1-treated groups compared to the

TBI+vehicle group (Fig. 2H). Analysis of the percentage of time spent in the target quadrant revealed that TBI significantly reduced this measure, whereas treatment with either CBD or Lip-1 effectively reversed this deficit (Fig. 2I). In the tail suspension test, mice in the CBD and Lip-1 groups exhibited increased struggle time, indicating reduced depressive-like behavior following TBI (Fig. 2E). Finally, hematoxylin staining performed 21 days post-TBI revealed a significant reduction in lesion volume in the TBI+CBD group, similar to that observed in the TBI+Lip-1 group (Fig. 2J, K), further supporting the neuroprotective role of CBD.

Collectively, these findings indicate that CBD effectively attenuates synaptic injury, neuronal degeneration, and behavioral deficits in the cerebral cortex following TBI.

CBD exhibits anti-ferroptotic properties and attenuates TBI-induced ferroptosis

Recent studies have provided substantial evidence that ferroptosis—a form of regulated cell death characterized by iron overload and lipid peroxidation—plays a key role in the pathogenesis of TBI [39]. To assess whether CBD modulates ferroptosis, we evaluated several related indicators both *in vitro* and *in vivo*.

First, we established an *in vitro* ferroptosis model by treating HT-22 cells with RSL3. Fluorescent staining with Ferro-Orange and Mito-FerroGreen

revealed that, compared with the RSL3 group, the CBD-treated group showed a notable reduction in Fe^{2+} fluorescence intensity in both the cytoplasm and mitochondria (Fig. 3B), suggesting suppression of iron accumulation. *In vivo*, Prussian blue staining of brain sections revealed marked deposition of iron-containing sideroferritin particles in the cortex one day after TBI. This iron overload was alleviated following treatment with CBD or Lip-1 (Fig. 3A). Furthermore, Western blotting analysis showed that TBI led to increased expression of transferrin receptor 1 (TfR1) and decreased expression of ferritin heavy chain (Fth) one day post-injury. Treatment with CBD or Lip-1 mitigated these alterations, helping to maintain iron homeostasis (Fig. 4A, B). Immunofluorescence staining for ferroportin (Fpn) in neurons showed a reduction in Fpn expression after TBI, which was partially restored by CBD and Lip-1 treatment (Fig. 4D-F).

Next, we evaluated lipid peroxidation using BODIPY™ 581/591 C11 staining in HT-22 cells. CBD significantly reduced RSL3-induced lipid ROS accumulation (Fig. 3C). Additionally, transcriptomic analysis comparing the TBI+vehicle and TBI+CBD groups, followed by GSEA pathway enrichment analysis, revealed significant changes in lipid metabolism-related pathways (Supporting Material: Fig. S1). To further investigate the molecular mechanisms of lipid peroxidation, we analyzed

the expression of key proteins by Western blotting and immunofluorescence. The levels of acyl-CoA synthetase long-chain family member 4 (Acsl4), cyclooxygenase-2 (Cox-2), and 4-hydroxynonenal (4hne) were significantly upregulated one day after TBI. CBD and Lip-1 treatment markedly reversed the upregulation of these lipid peroxidation markers (Fig. 4A-C, F).

Finally, we assessed the expression of the glutathione antioxidant system components xCT and glutathione peroxidase 4 (Gpx4), both of which are crucial regulators of ferroptosis. TBI resulted in a downregulation of these proteins, while treatment with CBD, similar to Lip-1, restored their expression (Fig. 4A, B, E, F). Furthermore, we directly measured the GSH/GSSG ratio in the ipsilateral cortex. TBI induced a marked decrease in this ratio, indicating an impaired glutathione redox status. Administration of CBD significantly reversed the TBI-induced decline in the GSH/GSSG ratio (Supporting Material: Fig. S2), further supporting the protective effect of CBD on the glutathione-dependent antioxidant system.

Taken together, these findings suggest that CBD possesses anti-ferroptotic activity and effectively attenuates neuronal ferroptosis during the acute phase following TBI.

CBD restores calcium homeostasis and mitochondrial function via the TRPV1/MCU axis

Given the close association between ferroptosis and mitochondrial dysfunction, we first assessed the mitochondrial membrane potential in HT-22 cells using JC-1 staining. RSL3 treatment induced mitochondrial depolarization, as evidenced by increased JC-1 monomer fluorescence. CBD significantly reversed this effect, indicating its protective role in maintaining mitochondrial membrane potential (Fig. 5A). To further explore how CBD ameliorates mitochondrial dysfunction, we examined intracellular calcium dynamics. Using Fluo-4 AM and Rhod-2 AM probes to monitor cytosolic and mitochondrial Ca^{2+} levels, respectively, we found that RSL3 markedly elevated calcium signal intensity in both compartments of HT-22 cells (Fig. 5B). Treatment with CBD significantly suppressed the Ca^{2+} overload, demonstrating a stronger inhibitory effect than Lip-1 (Fig. 5B).

We next investigated the underlying mechanisms by examining the expression of calcium uptake-related proteins. TRPV1, a known molecular target of CBD, is reported to undergo rapid desensitization following CBD exposure, thereby reducing Ca^{2+} influx [40]. Western blotting analysis revealed a significant upregulation of TRPV1 in the cortex one day post-TBI, which was partially attenuated by CBD treatment (Fig. 5C, D). To

validate the functional role of TRPV1, we knocked down TRPV1 in HT-22 cells using siRNA and subsequently treated the cells with RSL3. Fluo-4 AM staining showed that TRPV1 silencing mimicked the effect of CBD, significantly reducing cytoplasmic Ca^{2+} accumulation (Supporting Material: Fig. S3A).

As a key regulator of mitochondrial calcium uptake, MCU is implicated in RSL3-induced mitochondrial Ca^{2+} overload [42]. Western blotting analysis of cortical tissues and HT-22 cells demonstrated increased MCU expression following both TBI and RSL3 exposure. Treatment with CBD, as well as TRPV1 knockdown, significantly attenuated MCU upregulation (Fig. 5C, E-G). Moreover, pharmacological inhibition of TRPV1 with Capsazepine in a separate set of mice revealed that TRPV1 blockade reduced MCU phosphorylation following TBI (Supporting Material: Fig. S4). In a parallel experiment, siRNA-mediated knockdown of MCU markedly inhibited the RSL3-induced increase in mitochondrial Ca^{2+} levels (Supporting Material: Fig. S3B).

Collectively, these findings suggest that CBD exerts protective effects on calcium homeostasis and mitochondrial function by modulating the TRPV1/MCU pathway. This mechanism likely contributes to the therapeutic benefits of CBD in the early phase of TBI.

MCU is a core regulator of ferroptosis following TBI

To further investigate how CBD regulates ferroptosis through calcium homeostasis, we first examined the cellular localization of MCU expression one day after TBI. Immunofluorescence staining of brain sections near the injury site revealed that MCU was predominantly co-localized with NeuN, a neuronal marker, but not with GFAP or Iba-1, markers of activated astrocytes and microglia, respectively (Supporting Material: Fig. S5). These results indicated that MCU expression after TBI is primarily neuronal.

To manipulate neuronal MCU expression, we constructed and validated two rAAV vectors: rAAV-hSyn-EGFP-5'miR-30a-shRNA(MCU)-3'-miR30a-WPRE for neuron-specific MCU knockdown, and rAAV-hSyn-MCU-EGFP-WPRE-hGH-polyA for neuron-specific MCU overexpression. The efficacy of both vectors was confirmed by Western blotting and immunofluorescence (Supporting Material: Fig. S6A-H). Following neuronal MCU knockdown via rAAV, we observed no significant changes in the sham group. However, in TBI mice, MCU knockdown markedly reduced hemosiderin deposition one day post-injury (Fig. 6D). Consistently, mitochondrial ferritin (FtMt) and ferritin heavy chain (Fth), two key proteins in iron metabolism, were significantly upregulated in the sh(MCU)-TBI group compared to the control TBI group

(Fig. 7A, B). Cellular Fe^{2+} levels, measured after RSL3 treatment *in vitro*, were also reduced in the RSL3+siMCU group relative to the RSL3 group alone (Fig. 6E), further confirming the role of MCU in regulating iron accumulation within the ferroptosis model.

Transcriptome analysis of cortical tissue from control TBI and sh(MCU)-TBI groups revealed significant differences in pathways associated with intracellular lipid metabolism, including arachidonic acid metabolism (Fig. 6A-C). Additionally, BODIPY™ 581/591 C11 staining demonstrated that lipid peroxidation and mitochondrial membrane potential (MMP) disruption induced by RSL3 were substantially suppressed in the siMCU group (Fig. 6F). Expression of lipid peroxidation-related proteins, such as Cox-2 and 4hne, was also attenuated in the sh(MCU)-TBI group (Fig. 7A, B). For the glutathione antioxidant system, knockdown of MCU increased the expression of xCT and Gpx4 compared to the control TBI group (Fig. 7A, B), suggesting enhanced resistance to ferroptosis.

To further validate the pro-ferroptotic role of MCU, we overexpressed MCU in neurons using rAAV. Western blotting results showed that MCU overexpression significantly increased TfR1 expression in both sham and TBI conditions relative to controls (Fig. 7C, D). Meanwhile, Fth expression was significantly decreased in the OE(MCU) group compared to controls

(Fig. 7C, D). Proteins associated with lipid peroxidation—including Acsl4, Cox-2, and 4hne—were markedly upregulated in the OE(MCU)-TBI group, while Gpx4 expression was significantly reduced in both sham and TBI mice overexpressing MCU (Fig. 7C, D).

Collectively, these results demonstrate that MCU plays a key role in regulating ferroptosis-related events—including iron metabolism, lipid peroxidation, and antioxidant defense—in neurons following TBI. However, it is important to note that our analysis focused specifically on ferroptosis-associated markers; other cell death pathways (e.g., apoptosis and autophagy) were not examined in the MCU knockdown groups (Supporting Material: Fig. S7). Therefore, the conclusion that MCU is a core regulator of ferroptosis is limited to the ferroptosis-specific parameters measured in this study.

Neuronal MCU knockdown attenuates TBI-induced neuronal damage and behavioral deficits

To assess the protective effect of MCU knockdown on neuronal integrity, Fluoro-Jade B and Nissl staining were performed on brain sections from mice injected with rAAV. Compared to the control-TBI group, the sh(MCU)-TBI group exhibited a marked reduction in degenerating neurons and showed less cytoplasmic and nuclear atrophy (Fig. 8A, B). In addition, Western blotting analysis revealed that MCU knockdown reversed the TBI-

induced reductions in psd-95 and BDNF expression, suggesting improved synaptic integrity and neurotrophic support (Fig. 8C, E, F).

We further evaluated the impact of neuronal MCU knockdown on functional recovery after TBI. Behavioral tests were conducted following the establishment of the TBI model 21 days after rAAV injection, including the wire grip test, open field test, MWM, and tail suspension test (Fig. 9A). In the wire grip test conducted on days 1-5 post-TBI, both the control-sham group and sh(MCU)-sham group demonstrated initial motor recovery by day 1. However, the sh(MCU)-TBI group showed a significantly faster improvement in motor performance than the control-TBI group (Fig. 9B). Following motor recovery, an open field test was performed. The control-TBI group showed a significant decrease in central locomotor activity compared to the control-sham group, whereas the sh(MCU)-TBI group exhibited a significant increase in central distance relative to the control-TBI group, indicating alleviation of anxiety-like behavior (Fig. 9C, D). Between days 9 and 13 post-TBI, the Morris water maze test was conducted. The control-TBI group demonstrated significantly longer escape latencies than the sham group across all testing days, while the sh(MCU)-TBI group exhibited a faster learning curve and shorter escape latency compared to the control-TBI group (Fig. 9F, G). On the final testing day, the number of platform crossings within 90 seconds was significantly

higher in the sh(MCU)-TBI group than in the control-TBI group, reflecting improved spatial memory (Fig. 9H). Analysis of the percentage of time spent in the target quadrant revealed that TBI significantly reduced this measure, whereas neuronal MCU knockdown effectively reversed this deficit (Fig. 9I). In the tail suspension test conducted on day 15, mice in the control-TBI group exhibited a significant reduction in struggle time compared to the sham group, indicating depressive-like behavior. MCU knockdown restored the struggle time to a level closer to normal, suggesting an antidepressant-like effect (Fig. 9E).

Finally, on day 21 post-TBI, the mice used for behavioral tests were euthanized, and their brains were subjected to frozen sectioning to assess lesion volume. Quantitative analysis showed that the control-TBI group had significantly larger lesion volumes than the other three groups, including the sh(MCU)-TBI group, confirming the neuroprotective effect of MCU knockdown (Fig. 9K).

Collectively, these findings suggest that neuron-specific MCU knockdown exerts beneficial effects on neural repair and functional recovery following TBI, comparable to the therapeutic efficacy observed with CBD treatment.

CBD inhibits TBI-induced ferroptosis via the TRPV1/MCU/PI3K/Akt pathway

To explore the signaling mechanisms by which CBD regulates ferroptosis, we performed RNA extraction and transcriptome analysis on cortical tissue surrounding the injury site from both the control-TBI and sh(MCU)-TBI groups. Differentially expressed genes (DEGs) were subjected to KEGG pathway enrichment analysis. An identical KEGG analysis was conducted on DEGs from the TBI+vehicle and TBI+CBD groups. Interestingly, both analyses revealed a commonly enriched pathway, the PI3K-Akt signaling pathway (Fig. 6B, Fig. 10A).

Given that the PI3K/Akt pathway has been widely reported to suppress ferroptosis in various models, we next examined its potential role in CBD-mediated neuroprotection following TBI. Western blotting analysis showed that protein levels of PI3K and Akt were significantly decreased in the cortex one day post-TBI. However, CBD treatment significantly restored the expression of both proteins compared to the TBI+vehicle group (Fig. 10B, C). To further clarify the relationship between MCU and the PI3K/Akt pathway, we evaluated PI3K and Akt levels in the sh(MCU)-TBI group. Knockdown of MCU resulted in a significant upregulation of PI3K expression compared to the control-TBI group (Fig. 10F, G). Akt levels also showed an increasing trend in the sh(MCU)-TBI group,

although this change did not reach statistical significance (Fig. 10F, G).

To directly test whether MCU functions upstream of the PI3K/Akt pathway, we performed an independent experiment using the selective MCU inhibitor Ru360. As shown in Supporting Material Fig. S8, Ru360 treatment significantly increased the levels of phosphorylated PI3K (p-PI3K) and phosphorylated Akt (p-Akt) compared with the TBI+vehicle group, without markedly altering total PI3K or total Akt expression. These results indicate that pharmacological inhibition of MCU enhances PI3K/Akt signaling activation, supporting a hierarchical relationship in which MCU negatively regulates this pathway following TBI.

To determine whether PI3K activation is functionally required for the protective effects of CBD, we performed a rescue experiment using the PI3K inhibitor GDC-0941. Compared with the TBI+CBD group, PI3K inhibition led to decreased BDNF levels, increased psd-95 and Acsl4 levels, as well as decreased Fth and Gpx4 levels (Supporting Material: Fig. S9). These results indicate that blocking PI3K attenuates both the neuroprotective and anti-ferroptotic actions of CBD.

These findings suggest that CBD inhibits TBI-induced ferroptosis, at least in part, through the TRPV1/MCU/PI3K/Akt signaling axis.

Discussion

To date, investigations into the interplay between CBD and ferroptosis are extremely limited, especially under the pathological condition of TBI. Prior studies have predominantly centered on CBD's anti-inflammatory and antioxidant activities [43, 44], leaving its potential to ameliorate TBI-induced neuronal injury via ferroptosis modulation largely unexplored. In this work, we propose for the first time that CBD may attenuate neuronal damage and cognitive deficits following TBI by regulating ferroptosis, and we delineate its underlying mechanisms. At the mechanistic level, our findings indicate that CBD interacts with its established target TRPV1 as well as the mitochondrial calcium uniporter MCU to orchestrate a Ca^{2+}-centric regulation of ferroptosis in the aftermath of TBI. Importantly, by both silencing and overexpressing MCU, we directly link mitochondrial Ca^{2+} overload to the initiation of ferroptosis in our TBI model, thereby shedding light on the intricate crosstalk among intracellular ions.

Previous studies have elucidated the fundamental triggers of ferroptosis following TBI—namely, disrupted iron metabolism, dysregulated lipid peroxidation, and impairment of the glutathione antioxidant system [45]. Given CBD's multitarget profile and its demonstrated efficacy across various neurodisorder models [26], we sought to determine whether CBD could mitigate ferroptosis in TBI. Accordingly, mice received

intraperitoneal CBD post-TBI, and we evaluated key ferroptosis markers using Western blotting. CBD treatment markedly reversed TBI-induced alterations in iron-handling proteins, suppressed lipid peroxidation indicators, and restored glutathione system components (Fig. 4A–F), implying that CBD intervenes at multiple nodes within ferroptotic pathways. To validate these biochemical findings, we performed enhanced Perls' Prussian blue staining on brain sections, quantified intracellular Fe^{2+} in HT-22 cells, and carried out lipid ROS assays. All three assays confirmed that CBD significantly reduced iron accumulation and lipid ROS production (Fig. 3), paralleling the effects of Lip-1 and suggesting convergence on shared anti-ferroptotic targets. Building on previous reports of CBD's reparative effects in TBI [46], we next assessed synapse-related proteins by Western blotting and conducted targeted histological staining. CBD elevated BDNF expression and normalized psd-95 levels, and both Nissl and FJB staining demonstrated attenuated neuronal damage (Fig. 1A-D). Finally, in a separate cohort subjected to comprehensive behavioral analyses, CBD administration partially rescued deficits in motor coordination and memory, and alleviated anxiety- and depression-like behaviors when compared to the TBI + vehicle group (Fig. 2E-J). Together, these data detail CBD's anti-ferroptotic, neuroprotective, and cognitive-restorative actions in TBI, highlighting its potential to

counteract neuronal and behavioral impairments by suppressing ferroptosis. Interestingly, cannabinol (CBN) can improve synaptic and mitochondrial functions and alleviate cognitive decline. This is highly consistent with the protective effects of CBD on mitochondria and synapses that we observed in this study [47].

To further elucidate CBD's mechanism of action, mitochondrial involvement warrants examination given the organelle's central role in ferroptosis. Mitochondria contribute critically to ferroptosis by serving as primary sites for ROS generation, regulating fatty acid synthesis via ATP production control, hosting the DHODH anti-ferroptosis system, and interacting with antioxidants like NRF2 [48]. To assess CBD's impact on mitochondrial integrity, we first performed JC-1 staining in HT-22 cells. RSL3 exposure caused a marked loss of mitochondrial membrane potential, whereas co-treatment with CBD largely reinstated the red/green fluorescence ratio toward control levels (Fig. 5A). After initially identifying the modulatory effect of CBD on mitochondrial function, we next explored the ion channels that might contribute to changes in mitochondrial membrane potential. Given that several known CBD-associated receptors are involved in intracellular Ca^{2+} regulation, we employed Fluo-4 AM and Rhod-2 AM fluorescent probes to quantify changes in cytosolic and mitochondrial Ca^{2+} levels in HT-22 cells. RSL3

exposure elicited pronounced elevations in both compartments, whereas CBD co-treatment markedly attenuated these Ca^{2+} increases (Fig. 5B). TRPV1 has recently emerged as a prominent CBD target and serves as a key mediator of Ca^{2+} influx in the hippocampus [49]. To assess its regulation in the cortex, we quantified TRPV1 protein levels by Western blotting. Relative to sham, the TBI + vehicle group exhibited a pronounced upregulation of TRPV1, whereas CBD administration brought TRPV1 abundance back toward baseline (Fig. 5C, D).To directly test TRPV1's role in calcium handling, we applied siRNA to silence TRPV1 in HT-22 cells and then monitored cytosolic Ca^{2+} using the Fluo-4 AM probe. Cells lacking TRPV1 showed substantially lower RSL3-induced Ca^{2+} overload compared to cells treated with RSL3 alone (Supporting Material: Fig. S3A), demonstrating that TRPV1 is a critical conduit for pathological Ca^{2+} entry in this context. The dynamic regulation of mitochondrial Ca^{2+} is tightly linked to overall mitochondrial function. Previous studies have demonstrated that MCU mediates altered Ca^{2+} handling in TBI models, contributing to disrupted calcium homeostasis [50]. Emerging evidence suggests that the regulation of mitochondrial Ca^{2+} by MCU plays a pivotal role in modulating neuronal ferroptosis [29]. In our study, we first evaluated the expression of MCU in the cortical tissue of mice across different experimental groups. One day post-TBI, a marked increase in

MCU protein levels was observed, whereas treatment with either CBD or Lip-1 significantly attenuated this upregulation (Fig. 5C, D). To further validate MCU's functional role, we knocked down MCU in HT-22 cells using siRNA and assessed mitochondrial Ca^{2+} levels via Rhod-2 AM staining. The results revealed that MCU knockdown markedly reduced the RSL3-induced mitochondrial Ca^{2+} overload (Supporting Material: Fig. S3B), suggesting that MCU is essential for mediating mitochondrial Ca^{2+} dysregulation under ferroptotic stress. Additionally, to determine the relationship between MCU and TRPV1, we conducted Western blotting on HT-22 cells divided into four groups: control, si-TRPV1, RSL3, and RSL3 + si-TRPV1. Notably, MCU expression was significantly decreased in both TRPV1 knockdown groups, indicating that MCU may act downstream of TRPV1 in the signaling cascade (Fig. 10D, E). Collectively, these findings suggest that suppression of mitochondrial dysfunction and Ca^{2+} overload constitutes a key mechanism by which CBD mitigates TBI-induced ferroptosis. Furthermore, MCU appears to function as a critical molecular link between Ca^{2+} signaling and ferroptotic cell death in the post-TBI context.

To further elucidate the link between MCU and post-TBI ferroptosis, we utilized rAAV-mediated injection into the cerebral cortex to assess its role in neurons. Both knockdown and overexpression of MCU were performed

to evaluate their effects on ferroptosis. The results demonstrated that MCU knockdown did not significantly alter the expression of ferroptosis-related proteins in the sham group, whereas in the TBI group, MCU knockdown markedly alleviated ferroptosis, while its overexpression further exacerbated the condition (Fig. 7A-D). We next assessed whether silencing MCU could mitigate neuronal degeneration and damage. Enhanced Perls' Prussian blue staining and Nissl staining indicated that MCU knockdown attenuated TBI-induced neuronal injury and nuclear pyknosis (Fig. 8A, B, D). In addition, Western blotting showed that MCU knockdown reversed the downregulation of synaptic marker psd-95 and neurotrophic factor BDNF following TBI, suggesting protection against synaptic damage and trophic decline (Fig. 8C, E, F). Behavioral outcomes were also evaluated in mice subjected to rAAV injection. MCU knockdown accelerated motor function recovery after TBI. The Morris water maze test revealed that mice in the sh(MCU)-TBI group exhibited less memory impairment. Furthermore, silencing MCU alleviated TBI-induced depressive- and anxiety-like behaviors (Fig. 9A-I). Based on these findings, we sought to further explore how MCU regulates ferroptosis following TBI. To identify potential signaling pathways involved, we performed KEGG analysis on DEGs from both TBI+vehicle vs TBI+CBD groups and control-TBI vs sh(MCU)-TBI groups. The PI3K/Akt signaling pathway was significantly

and consistently enriched as the shared differentially enriched pathway in both datasets (Fig. 6B, Fig. 10A). In our previous work, we identified the PI3K/Akt pathway as a critical mediator in suppressing neuronal ferroptosis after TBI [30]. Western blotting confirmed that p-PI3K and p-Akt levels were significantly reduced in the control-TBI group, while MCU knockdown reversed this reduction (Fig. 10F, G). Similarly, in the TBI+CBD group, the expression of p-PI3K and p-Akt showed a comparable upregulation to that observed in the MCU knockdown group (Fig. 10B, C). Taken together, these findings lead us to propose that the neuroprotective and anti-ferroptotic effects of CBD in TBI may be mediated, at least in part, via the TRPV1/MCU/PI3K/Akt signaling axis (Fig. 10A-G).

In summary, our study suggests that CBD functions not only as a neuroprotective agent but also as a novel regulator of ferroptosis. The TRPV1/MCU/PI3K/Akt axis mediated by CBD may serve as a potential therapeutic target for ferroptosis following TBI. These conclusions are supported by four key findings (Fig. 11). First, CBD and Lip-1 exhibited comparable inhibitory effects on ferroptosis-related neuronal damage induced by TBI in mice. Second, CBD suppressed TRPV1/MCU-mediated cytosolic and mitochondrial Ca^{2+} overload, thereby preventing mitochondrial dysfunction and ROS accumulation. Third, both knockdown

and overexpression of MCU revealed bidirectional regulation of ferroptosis, underscoring its central role in neuroprotection. Fourth, CBD treatment and targeted knockdown of key pathway components demonstrated significant modulation of downstream molecular events. Despite these promising findings, several limitations remain. This study has certain limitations in the detection of intracellular Ca^{2+} levels: while Fig. 5B shows that CBD treatment reduces Ca^{2+} levels, the static imaging approach employed fails to capture the temporal dynamics required for elucidating the process of MCU-mediated mitochondrial Ca^{2+} overload. Due to time and experimental constraints, this study was unable to conduct time-lapse Ca^{2+} imaging experiments. Thus, we further elaborate on this limitation and plan to introduce dynamic Ca^{2+} imaging technology in subsequent studies to more comprehensively elucidate the regulatory effect of CBD on Ca^{2+} signaling pathways. The effects of CBD on glial cells and neuroimmune interactions were not extensively explored, and the crosstalk between Ca^{2+} and Fe^{2+} warrants further investigation. Future studies employing conditional knockout models may help elucidate the cellular sources and translational potential of CBD's protective actions.

Abbreviations

ANOVA analysis of variance

CBD cannabidiol

CCI	controlled cortical impact
DEGs	differentially expressed genes
GO	Gene Ontology
GSEA	Gene Set Enrichment Analysis
KEGG	Kyoto Encyclopedia of Genes and Genomes
Lip-1	Liproxstatin-1
ROS	reactive oxygen species
MCU	mitochondrial calcium uniporter
MWM	Morris Water Maze
PI3K/Akt	phosphoinositide 3-kinase/protein kinase B
rAAV	recombinant adeno-associated viruses
SD	standard deviation
TBI	Traumatic brain injury
TRPV1	transient receptor potential vanilloid type 1.

Supplementary materials

Original uncropped images of Western blot (WB).

Supporting Material: Table S1. Sequence of si-RNA and rAAV; Table S2. Primary and secondary antibodies used for Western blotting (WB); Fig. S1. Transcriptomic analysis comparing TBI-vehicle and TBI-CBD groups; Fig. S2 The effect of CBD on the GSH/GSSG ratio in the cerebral cortex of mice after TBI. Fig. S3. Cytosolic and mitochondrial Ca^{2+} levels after siRNA treatment. Fig. S4. The effect of TRPV1 inhibition on the phosphorylation of MCU. Fig. S5. Cellular localization of MCU in the cortex at 1 day post-TBI. Fig. S6. rAAV-mediated knockdown and overexpression of *MCU*. Fig. S7. The effect of *MCU* knockdown on TBI-induced apoptosis and autophagy. Fig. S8. The effects of MCU inhibition on the PI3K/Akt pathway and ferroptosis. Fig. S9. The influence of PI3K inhibition on the neuroprotective effect and anti-ferroptosis effect of CBD.

Author contributions

C.L., T.W., and Q.L. performed study concept and design. Y.X., X.L., Z.G., X.C., Y.Z., and B.J. performed animal experiments and cell experiments. Y.X., X.L., Z.G., Y.W., R.W., Q.L., T.W., and C.L. provided the statistical analysis. Y.X. wrote the original draft. X.L., Q.L., T.W., and C.L. critically reviewed and offered insights for this manuscript. All authors read and approved the final manuscript.

Funding

This work was supported by the National Natural Science Foundation of China (82460256, 82271409), Yunnan Provincial Key Project for Basic Research Program (202501AS070020), and National Training Program of Innovation and Entrepreneurship for Undergraduate (202510678024).

Declaration of competing interest

The authors declare that they have no known competing financial interests or personal relationships that could have appeared to influence the work reported in this paper.

Availability of data and materials

The data that support the findings of this study are available from the corresponding author, Chengliang Luo, upon request.

Declarations

Ethics approval and consent to participate

All the animal procedures were approved by the Institutional Animal Care Committee of Kunming Medical University on 4 Mar 2024 (approval no. kmmu20240775). The Local Ethics Committee acts in accordance with the International Council for Laboratory Animal Science (ICLAS).

Consent for publication

All authors gave their consent for publication.

Competing interests

The authors declare no competing interests.

References

1. Maas AIR, Menon DK, Manley GT, Abrams M, Akerlund C, Andelic N, Aries M, Bashford T, Bell MJ, Bodien YG *et al*: **Traumatic brain injury: progress and challenges in prevention, clinical care, and research**. *Lancet Neurol* 2022, **21**(11):1004-1060.
2. Malhotra AK, Jaffe RH, Shakil H, Mathieu F, Nathens AB, Kulkarni AV, Diep C, Yuan EY, Ladha KS, Coyte PC *et al*: **Unemployment and Personal Income Loss After Traumatic Brain Injury**. *Jama Surg* 2024, **159**(12):1415-1422.
3. Blennow K, Brody DL, Kochanek PM, Levin H, McKee A, Ribbers GM, Yaffe K, Zetterberg H: **Traumatic brain injuries**. *Nat Rev Dis Primers* 2016, **2**.
4. Brody DL, Chan L, Cizza G: **How do you treat traumatic brain injury? One symptom at a time**. *Ann Neurol* 2019, **86**(3):329-331.
5. Hassett L: **Physiotherapy management of moderate-to-severe**

traumatic brain injury. *J Physiother* 2023, **69**(3):141-147.

6. Sobue A, Komine O, Endo F, Kakimi C, Miyoshi Y, Kawade N, Watanabe S, Saito Y, Murayama S, Saido TC *et al*: **Microglial cannabinoid receptor type II stimulation improves cognitive impairment and neuroinflammation in Alzheimer's disease mice by controlling astrocyte activation**. *Cell Death Dis* 2024, **15**(11):858.

7. Shohami E, Novikov M, Mechoulam R: **A nonpsychotropic cannabinoid, HU-211, has cerebroprotective effects after closed head injury in the rat**. *J Neurotrauma* 1993, **10**(2):109-119.

8. Shohami E, Novikov M, Bass R: **Long-term effect of HU-211, a novel non-competitive NMDA antagonist, on motor and memory functions after closed head injury in the rat**. *Brain Res* 1995, **674**(1):55-62.

9. Shohami E, Gallily R, Mechoulam R, Bass R, Ben-Hur T: **Cytokine production in the brain following closed head injury: dexanabinol (HU-211) is a novel TNF-alpha inhibitor and an effective neuroprotectant**. *J Neuroimmunol* 1997, **72**(2):169-177.

10. Knoller N, Levi L, Shoshan I, Reichenthal E, Razon N, Rappaport ZH, Biegon A: **Dexanabinol (HU-211) in the treatment of severe closed head injury: a randomized, placebo-controlled, phase II**

clinical trial. *Crit Care Med* 2002, **30**(3):548-554.

11. Maas AI, Murray G, Henney H, 3rd, Kassem N, Legrand V, Mangelus M, Muizelaar JP, Stocchetti N, Knoller N, Pharmos TBIi: **Efficacy and safety of dexanabinol in severe traumatic brain injury: results of a phase III randomised, placebo-controlled, clinical trial**. *Lancet Neurol* 2006, **5**(1):38-45.
12. Bonini SA, Premoli M, Tambaro S, Kumar A, Maccarinelli G, Memo M, Mastinu A: **: A comprehensive ethnopharmacological review of a medicinal plant with a long history**. *J Ethnopharmacol* 2018, **227**:300-315.
13. Tham M, Yilmaz O, Alaverdashvili M, Kelly MEM, Denovan-Wright EM, Laprairie RB: **Allosteric and orthosteric pharmacology of cannabidiol and cannabidiol-dimethylheptyl at the type 1 and type 2 cannabinoid receptors**. *Brit J Pharmacol* 2019, **176**(10):1455-1469.
14. Wang X, Lin C, Jin S, Wang YB, Peng YH, Wang XH: **Cannabidiol alleviates neuroinflammation and attenuates neuropathic pain via targeting FKBP5**. *Brain Behav Immun* 2023, **111**:365-375.
15. Wang HW, Yang GM, Zhang XX, Zhang HJ, Liu Y, Wang C, Miao L, Li Y, Huang YZ, Teng HX *et al*: **Cannabidiol protects the liver**

from α-Amanitin-induced apoptosis and oxidative stress through the regulation of Nrf2. *Food Chem Toxicol* 2023, **182**.

16. Aychman MM, Goldman DL, Kaplan JS: **Cannabidiol's neuroprotective properties and potential treatment of traumatic brain injuries**. *Front Neurol* 2023, **14**:1087011.

17. Lins BR, Anyaegbu CC, Hellewell SC, Papini M, McGonigle T, De Prato L, Shales M, Fitzgerald M: **Cannabinoids in traumatic brain injury and related neuropathologies: preclinical and clinical research on endogenous, plant-derived, and synthetic compounds**. *J Neuroinflammation* 2023, **20**(1):77.

18. Devinsky O, Marsh E, Friedman D: **Cannabidiol in patients with treatment-resistant epilepsy: an open-label interventional trial (vol 15, pg 270, 2016)**. *Lancet Neurology* 2016, **15**(4):352-352.

19. Dixon SJ, Lemberg KM, Lamprecht MR, Skouta R, Zaitsev EM, Gleason CE, Patel DN, Bauer AJ, Cantley AM, Yang WS *et al*: **Ferroptosis: An Iron-Dependent Form of Nonapoptotic Cell Death**. *Cell* 2012, **149**(5):1060-1072.

20. Geng ZW, Guo ZL, Guo RB, Ye RD, Zhu WS, Yan B: **Ferroptosis and traumatic brain injury**. *Brain Research Bulletin* 2021, **172**:212-219.

21. Liu Y, Zhao Z, Guo J, Ma Y, Li J, Ji H, Chen Z, Zheng J:

Anacardic acid improves neurological deficits in traumatic brain injury by anti-ferroptosis and anti-inflammation. *Exp Neurol* 2023, **370**:114568.

22. Liang Z, Candib A, Soriano-Castell D, Fischer W, Finley K, Maher P: **Fragment-based drug discovery and biological evaluation of novel cannabinol-based inhibitors of oxytosis/ferroptosis for neurological disorders**. *Redox Biol* 2024, **72**:103138.

23. Xu YJ, Jia BW, Li J, Li QQ, Luo CL: **The Interplay between Ferroptosis and Neuroinflammation in Central Neurological Disorders**. *Antioxidants-Basel* 2024, **13**(4).

24. Liu DH, Yang S, Yu SG: **Interactions Between Ferroptosis and Oxidative Stress in Ischemic Stroke**. *Antioxidants-Basel* 2024, **13**(11).

25. Iftinca M, Defaye M, Altier C: **TRPV1-Targeted Drugs in Development for Human Pain Conditions**. *Drugs* 2021, **81**(1):7-27.

26. Bih CI, Chen T, Nunn AVW, Bazelot M, Dallas M, Whalley BJ: **Molecular Targets of Cannabidiol in Neurological Disorders**. *Neurotherapeutics* 2015, **12**(4):699-730.

27. Liu LP, Sun XD, Guo YL, Ge KL: **Evodiamine induces ROS-Dependent cytotoxicity in human gastric cancer cells via**

TRPV1/Ca

pathway. *Chem-Biol Interact* 2022, **351**.

28. Kamer KJ, Mootha VK: **The molecular era of the mitochondrial calcium uniporter**. *Nat Rev Mol Cell Bio* 2015, **16**(9):545-553.

29. Marmolejo-Garza A, Krabbendam IE, Luu MDA, Brouwer F, Trombetta-Lima M, Unal O, O'Connor SJ, Majerníková N, Elzinga CRS, Mammucari C *et al*: **Negative modulation of mitochondrial calcium uniporter complex protects neurons against ferroptosis**. *Cell Death & Disease* 2023, **14**(11).

30. Cheng Y, Gao Y, Li J, Rui TY, Li QQ, Chen H, Jia BW, Song YT, Gu ZY, Wang T *et al*: **TrkB agonist N-acetyl serotonin promotes functional recovery after traumatic brain injury by suppressing ferroptosis via the PI3K/Akt/Nrf2/ Ferritin H pathway**. *Free Radical Bio Med* 2023, **194**:184-198.

31. Wang JM, Xu HM, Cheng XF, Yang JR, Yan ZP, Ma HL, Zhao YF, Ommati MM, Manthari RK, Wang JD: **Calcium relieves fluoride-induced bone damage through the PI3K/AKT pathway**. *Food Funct* 2020, **11**(1):1155-1164.

32. Mori MA, Meyer E, Soares LM, Milani H, Guimaraes FS, de Oliveira RMW: **Cannabidiol reduces neuroinflammation and promotes neuroplasticity and functional recovery after brain**

ischemia. *Prog Neuro-Psychoph* 2017, **75**:94-105.

33. Li J, Jia BW, Xu YJ, Zhao Y, Wang SW, Yang R, Su L, Zeng XF, Li QQ, Luo CL: **Inhibition of mitoNEET ameliorates traumatic brain injury-induced ferroptosis and cognitive dysfunction by stabilizing dihydroorotate dehydrogenase**. *Exp Neurol* 2025, **389**.

34. Xu BT, Li MF, Chen KC, Li X, Cai NB, Xu JP, Wang HT: **Mitofusin-2 mediates cannabidiol-induced neuroprotection against cerebral ischemia in rats**. *Acta Pharmacol Sin* 2023, **44**(3):499-512.

35. Yang HY, Hong Y, Gong MJ, Cai SH, Yuan ZW, Feng SL, Chen QB, Liu XX, Mei ZR: **Fisetin exerts neuroprotective effects and by inhibiting ferroptosis and oxidative stress after traumatic brain injury**. *Front Pharmacol* 2024, **15**.

36. Rui TY, Wang HC, Li QQ, Cheng Y, Gao Y, Fang XX, Ma XY, Chen G, Gao C, Gu ZY *et al*: **Deletion of in neurons counteracts the protective effect of melatonin against traumatic brain injury-induced ferroptosis**. *J Pineal Res* 2021, **70**(2).

37. Yin Y, Edelman GM, Vanderklish PW: **The brain-derived neurotrophic factor enhances synthesis of Arc in synaptoneurosomes**. *P Natl Acad Sci USA* 2002, **99**(4):2368-2373.

38. Béïque JC, Andrade R: **PSD-95 regulates synaptic transmission and plasticity in rat cerebral cortex**. *J Physiol-London* 2003, **546**(3):859-867.

39. Xie BS, Wang YQ, Lin Y, Mao Q, Feng JF, Gao GY, Jiang JY: **Inhibition of ferroptosis attenuates tissue damage and improves long-term outcomes after traumatic brain injury in mice**. *Cns Neurosci Ther* 2019, **25**(4):465-475.

40. Kossakowski R, Schlicker E, Toczek M, Weresa J, Malinowska B: **Cannabidiol Affects the Bezold-Jarisch Reflex via TRPV1 and 5-HT(3) Receptors and Has Peripheral Sympathomimetic Effects in Spontaneously Hypertensive and Normotensive Rats**. *Front Pharmacol* 2019, **10**:500.

41. Devinsky O, Jones NA, Cunningham MO, Jayasekera BAP, Devore S, Whalley BJ: **Cannabinoid treatments in epilepsy and seizure disorders**. *Physiol Rev* 2024, **104**(2).

42. Alevriadou BR, Patel A, Noble M, Ghosh S, Gohil VM, Stathopulos PB, Madesh M: **Molecular nature and physiological role of the mitochondrial calcium uniporter channel**. *Am J Physiol-Cell Ph* 2020, **320**(4):C465-C482.

43. Fouda MA, Fathy Mohamed Y, Fernandez R, Ruben PC: **Anti-inflammatory effects of cannabidiol against**

lipopolysaccharides in cardiac sodium channels. *Br J Pharmacol* 2022, **179**(24):5259-5272.

44. Casares L, Garcia V, Garrido-Rodriguez M, Millan E, Collado JA, Garcia-Martin A, Penarando J, Calzado MA, de la Vega L, Munoz E: **Cannabidiol induces antioxidant pathways in keratinocytes by targeting BACH1**. *Redox Biol* 2020, **28**:101321.

45. Wei ZQ, Yu HH, Zhao HJ, Wei MZ, Xing H, Pei JY, Yang Y, Ren KD: **Broadening horizons: ferroptosis as a new target for traumatic brain injury**. *Burns Trauma* 2024, **12**.

46. Friedman LK, Peng H, Zeman RJ: **Cannabidiol reduces lesion volume and restores vestibulomotor and cognitive function following moderately severe traumatic brain injury**. *Exp Neurol* 2021, **346**.

47. Dar NJ, Currais A, Taguchi T, Andrews N, Maher P: **Cannabinol (CBN) alleviates age-related cognitive decline by improving synaptic and mitochondrial health**. *Redox Biol* 2025, **84**:103692.

48. Li J, Jia YC, Ding YX, Bai J, Cao F, Li F: **The crosstalk between ferroptosis and mitochondrial dynamic regulatory networks**. *Int J Biol Sci* 2023, **19**(9):2756-2771.

49. Shen B, Yang G, Lv M, Wu Z, Zhang Y, Cao Y, Shu J, Dong W, Hou Z, Jing D *et al*: **Cannabidiol attenuates methamphetamine-**

induced oxidative neurotoxicity via regulating transient receptor potential vanilloid type 1. *Phytomedicine* 2025, **145**.

50. Zhang L, Wang HD, Zhou XM, Mao L, Ding K, Hu ZG: **Role of mitochondrial calcium uniporter-mediated Ca and iron accumulation in traumatic brain injury**. *J Cell Mol Med* 2019, **23**(4):2995-3009.

Figure legends

Fig. 1 CBD attenuated TBI-induced neuronal damage and degeneration. **A** Representative images of Fluoro-Jade B staining for neuronal injury and degeneration in different groups. Scale bar=100 μm. **B** Representative Nissl staining images showing neuronal morphological changes in different groups. Scale bar=100 μm. **C, E, F** Western blotting analysis of psd-95 and BDNF expression levels (n = 6). Uncropped Western blotting images were shown in Supplementary Materials. **D** The number of Fluoro-Jade B (FJB)-positive neurons. *$p < 0.05$, **$p < 0.01$; ***$p < 0.001$; ****$p < 0.0001$; ns, not significant.

Fig. 2 Effects of CBD on motor and cognitive dysfunction after TBI. **A** Schematic workflow of behavioral analysis and brain lesion volume analysis. **B** Wire-grip test assessing motor performance (n = 8). **C** Open

field test assessing locomotor activity. **D** Quantification of central distance traveled in the open field test (n = 8). **E** Immobility time in the tail suspension test (n = 8). **F** Representative images from the Morris water maze test. **G, H, I** Statistical analysis of the Morris water maze test (n = 8). **J** Representative H&E-stained brain sections at 21 days post-TBI in different groups. **K** Quantification of brain lesion volume at 21 days post-injury (n = 3). *$p < 0.05$, **$p < 0.01$, ***$p < 0.001$, ****$p < 0.0001$; ns, not significant.

Fig. 3 CBD modulated iron metabolism and lipid peroxidation after TBI. **A** Perls' Prussian blue staining of brain sections at 1 day post-injury in different groups. Scale bar = 100 μm. **B** Representative images of FerroOrange and Mito-FerroGreen staining in cells. Scale bar = 100 μm. **C** Representative images of BODIPY $^{581/591}$ C11 staining for lipid peroxidation in different groups. Scale bar = 100 μm.

Fig. 4 CBD reduced ferroptosis-associated markers following TBI. **A** Western blotting analysis of proteins related to the ferroptosis pathway in different groups (n = 6). Uncropped Western blotting images were shown in Supplementary Materials. **B** Quantification of protein expression levels in **A**, shown as mean ± SD. *$p < 0.05$, **$p < 0.01$, ***$p < 0.001$, ****$p < 0.0001$; ns, not significant. **C-E** Representative immunofluorescence images for 4hne, Fpn, and xCT in different groups. Scale bar: 100 μm. **F**

Quantification of fluorescence intensity, presented as mean ± SD.

Fig. 5 CBD regulated mitochondrial function and calcium homeostasis in cells. **A** JC-1 staining to evaluate mitochondrial membrane potential. Scale bar = 100 μm. **B** Fluorescence images showing cytosolic and mitochondrial Ca^{2+} levels in HT-22 cells under different treatments. Scale bar=100 μm. **C** Western blotting analysis of TRPV1 and MCU expression in different groups (n = 6). Uncropped Western blotting images were shown in Supplementary Materials. **D** Quantification of TRPV1 and MCU protein levels, shown as mean ± SD. *$p < 0.05$, ****$p < 0.0001$; ns, not significant.

Fig. 6 MCU knockdown reduced iron accumulation and lipid peroxidation after TBI. **A** Distribution of differentially expressed genes between the control-TBI and sh(MCU)-TBI groups. **B** KEGG enrichment analysis of differentially expressed genes. **C** GSEA analysis of lipid metabolism–related pathways.**D** Perls' Prussian blue staining of brain sections at 1 day post-injury in different groups. Scale bar = 100 μm.**E** Representative images of FerroOrange and Mito-FerroGreen staining in cells. Scale bar = 100 μm. **F** Representative image of BODIPY 581/591 C11 staining for lipid peroxidation. Scale bar = 100 μm.

Fig. 7 Effects of MCU knockdown and overexpression on ferroptosis after TBI. A Western blotting analysis of ferroptosis-related proteins after MCU knockdown in different groups (n = 6). Uncropped Western blotting images

were shown in Supplementary Materials. B, C Quantification of protein expression levels, shown as mean ± SD. *$p < 0.05$, **$p < 0.01$, ***$p < 0.001$, ****$p < 0.0001$; ns, not significant. D Western blotting analysis of ferroptosis-related proteins after MCU overexpression in different groups (n = 6). Uncropped Western blotting images are shown in Supplementary Materials.

Fig. 8 MCU knockdown alleviated TBI-induced neuronal injury and degeneration. **A** Representative FJB staining images indicating neuronal degeneration. Scale bar = 100 μm.**B** Nissl staining showing neuronal morphological changes in different groups. Scale bar = 100 μm. **C, E, F** Western blotting analysis of psd-95 and BDNF protein levels (n = 6). β-Tubulin served as the internal control. Uncropped Western blotting images were shown in Supplementary Materials. **D** The number of Fth-positive neurons. *$p < 0.05$, **$p < 0.01$,***$p < 0.001$; ns, not significant.

Fig. 9 MCU knockdown improved motor and cognitive performance after TBI. **A** Schematic timeline of behavioral and brain lesion volume analyses. **B** Wire-grip test for motor function (n = 8). **C** Open field test assessing locomotor activity (n = 8).**D** Quantification of central distance traveled in the open field test (n = 8). **E** Immobility time in the tail suspension test (n = 8). **F** Representative images from the Morris water maze test. **G, H, I** Statistical analysis of the Morris water maze test (n = 8). **J** H&E-stained

brain sections at 21 days post-injury. **J** Quantification of brain lesion volume at 21 days post-TBI (n = 3). *$p < 0.05$, **$p < 0.01$, ***$p < 0.001$, ****$p < 0.0001$; ns, not significant.

Fig. 10 CBD inhibited ferroptosis signaling pathways activated by TBI. **A** Top 25 significantly enriched KEGG pathways based on DEGs from transcriptomic analysis. **B, D, F** Western blotting bands of key pathway proteins (n = 6). Uncropped Western blotting images were shown in Supplementary Materials. **C, E, G** Quantification of protein levels, shown as mean ± SD. *$p < 0.05$, **$p < 0.01$, ****$p < 0.0001$; ns, not significant.

Fig. 11 Summary diagram of research results.

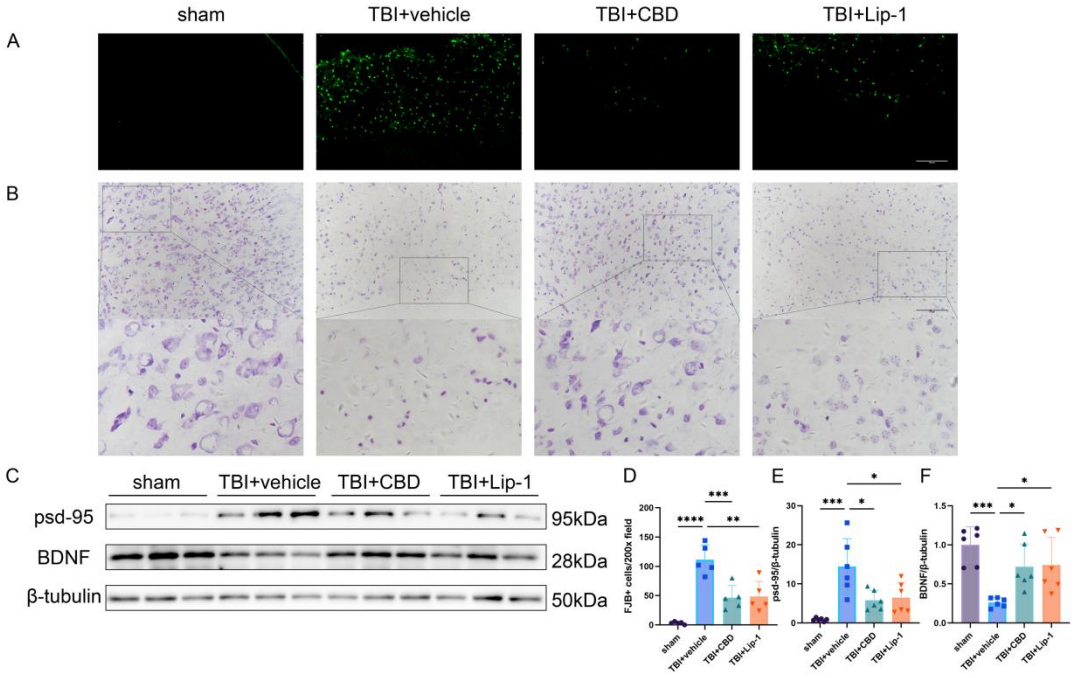

Fig. 1 CBD attenuated TBI-induced neuronal damage and degeneration. **A** Representative images of Fluoro-Jade B staining for neuronal injury and degeneration in different groups. Scale bar=100 μm. **B** Representative Nissl staining images showing neuronal morphological changes in different groups. Scale bar=100 μm. **C, E, F** Western blotting analysis of psd-95 and BDNF expression levels (n = 6). Uncropped Western blotting images were shown in Supplementary Materials. **D** The number of Fluoro-Jade B (FJB)-positive neurons. *$p < 0.05$, **$p < 0.01$; ***$p < 0.001$; ****$p < 0.0001$; ns, not significant.

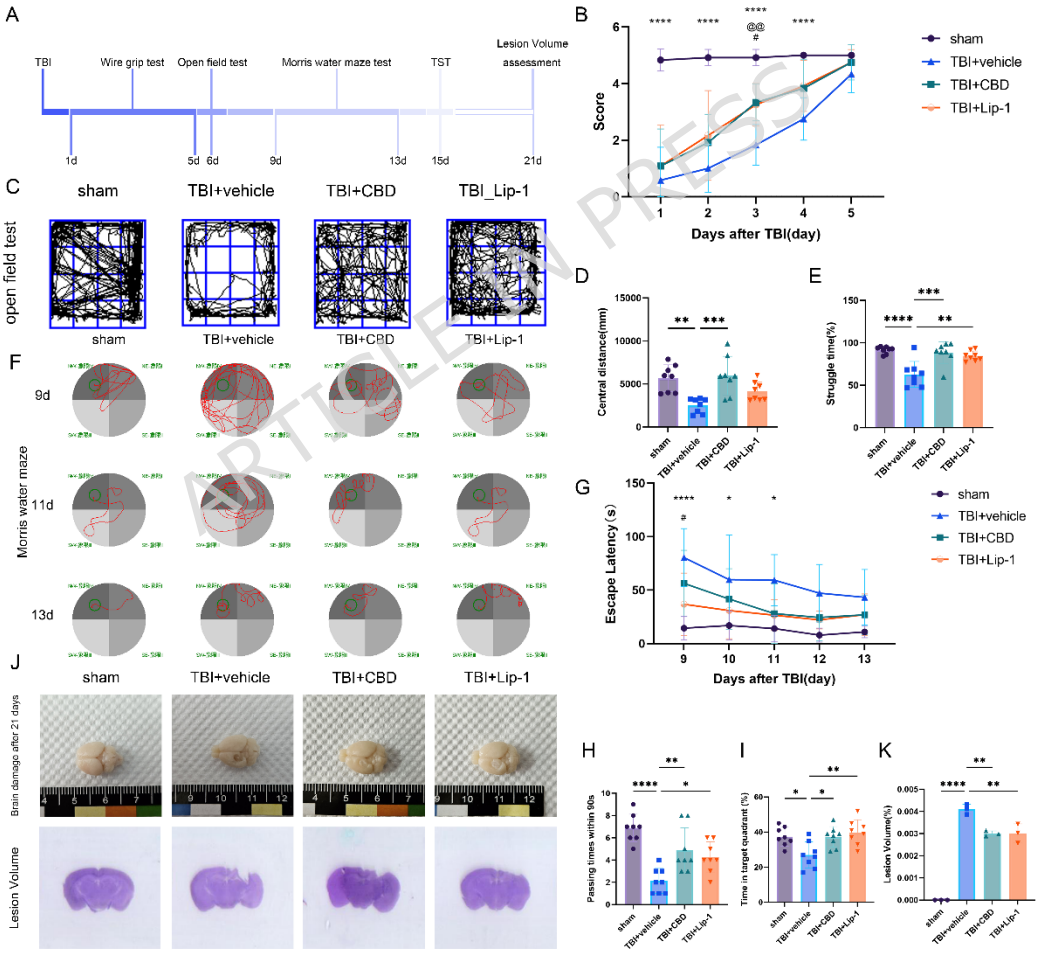

Fig. 2 Effects of CBD on motor and cognitive dysfunction after TBI. **A**

Schematic workflow of behavioral analysis and brain lesion volume analysis. **B** Wire-grip test assessing motor performance (n = 8). **C** Open field test assessing locomotor activity. **D** Quantification of central distance traveled in the open field test (n = 8). **E** Immobility time in the tail suspension test (n = 8). **F** Representative images from the Morris water maze test. **G, H, I** Statistical analysis of the Morris water maze test (n = 8). **J** Representative H&E-stained brain sections at 21 days post-TBI in different groups. **K** Quantification of brain lesion volume at 21 days post-injury (n = 3). *$p < 0.05$, **$p < 0.01$, ***$p < 0.001$, ****$p < 0.0001$; ns, not significant.

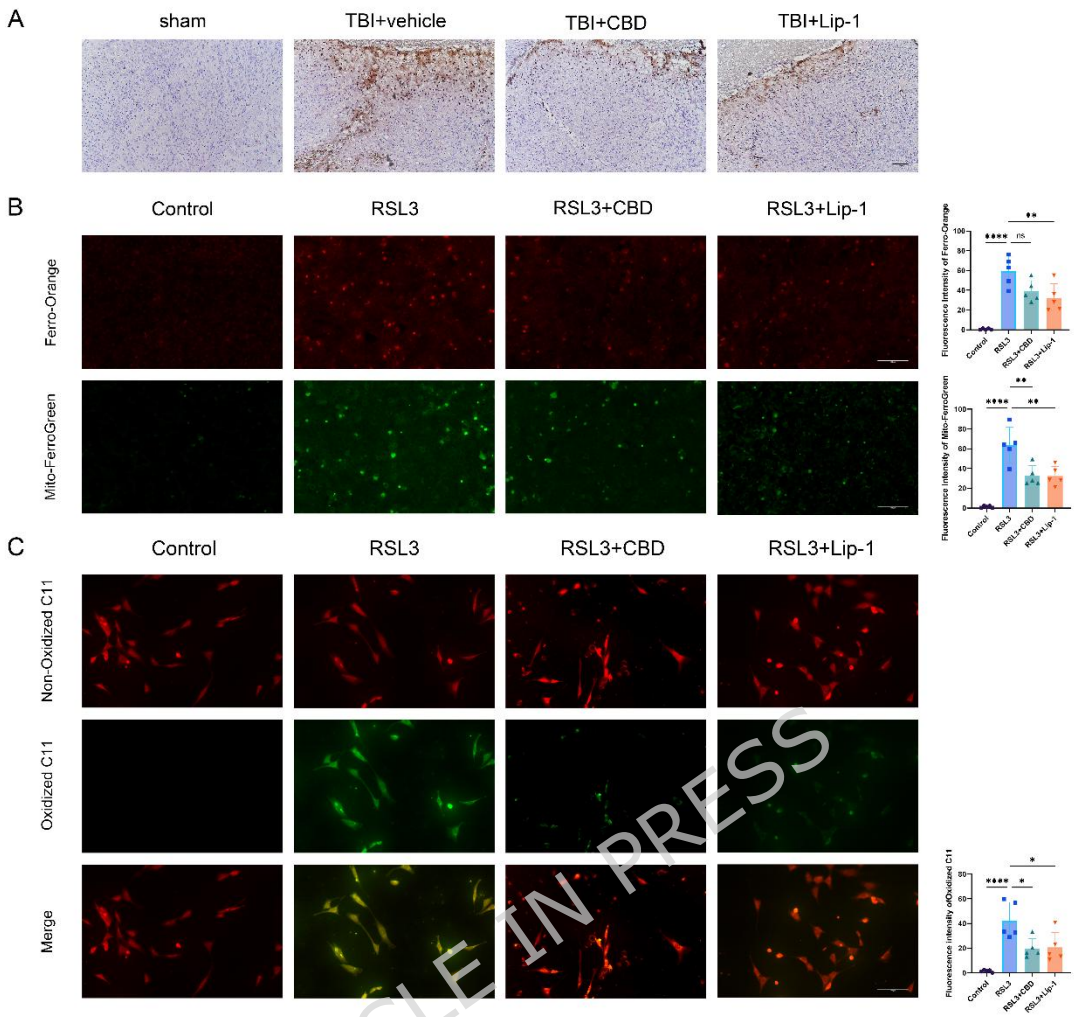

Fig. 3 CBD modulated iron metabolism and lipid peroxidation after TBI. **A** Perls' Prussian blue staining of brain sections at 1 day post-injury in different groups. Scale bar = 100 μm. **B** Representative images of FerroOrange and Mito-FerroGreen staining in cells. Scale bar = 100 μm. **C** Representative images of BODIPY $^{581/591}$ C11 staining for lipid peroxidation in different groups. Scale bar = 100 μm.

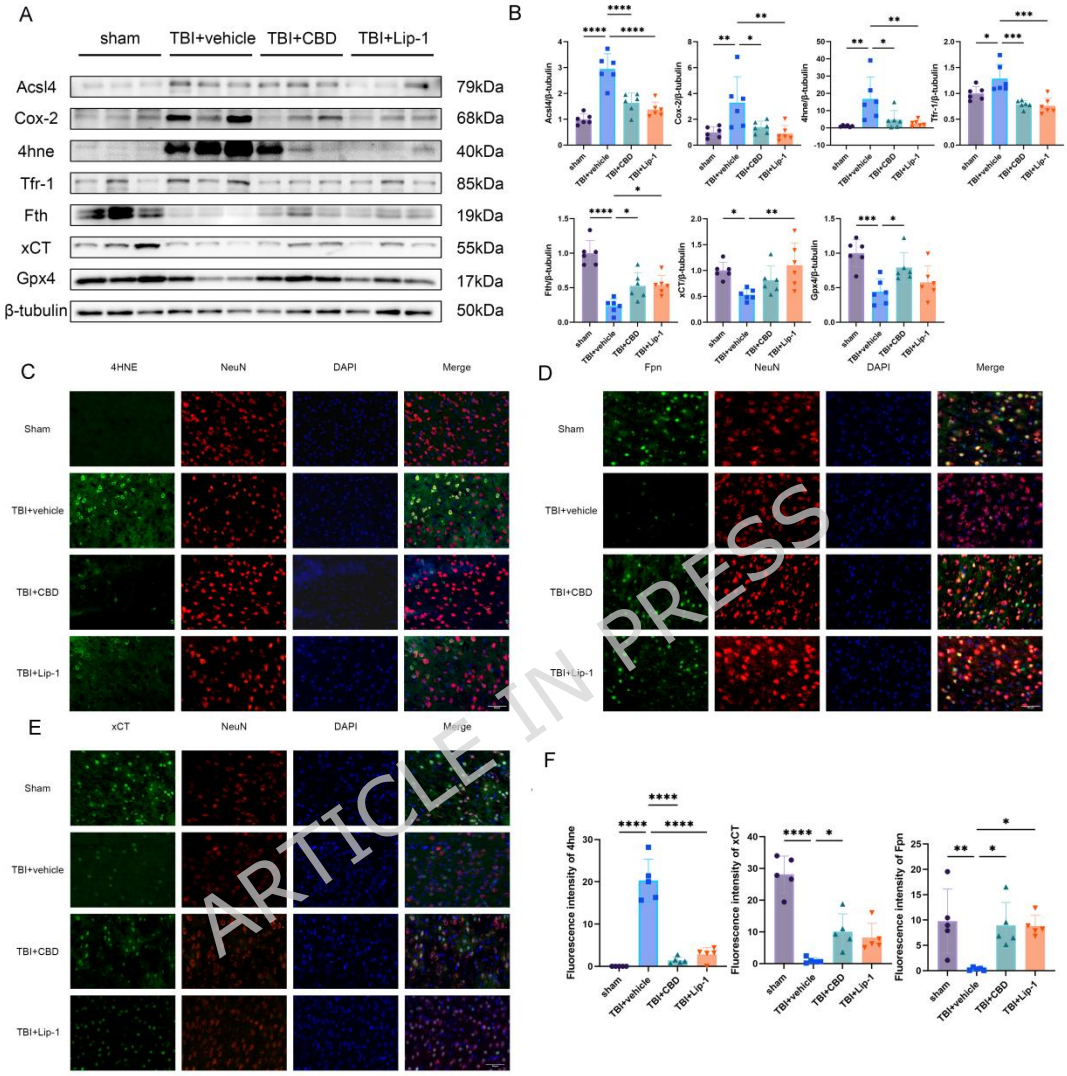

Fig. 4 CBD reduced ferroptosis-associated markers following TBI. **A** Western blotting analysis of proteins related to the ferroptosis pathway in different groups (n = 6). Uncropped Western blotting images were shown in Supplementary Materials. **B** Quantification of protein expression levels in **A**, shown as mean ± SD. *$p < 0.05$, **$p < 0.01$, ***$p < 0.001$, ****$p <$

0.0001; ns, not significant. **C-E** Representative immunofluorescence images for 4hne, Fpn, and xCT in different groups. Scale bar: 100 μm. **F** Quantification of fluorescence intensity, presented as mean ± SD.

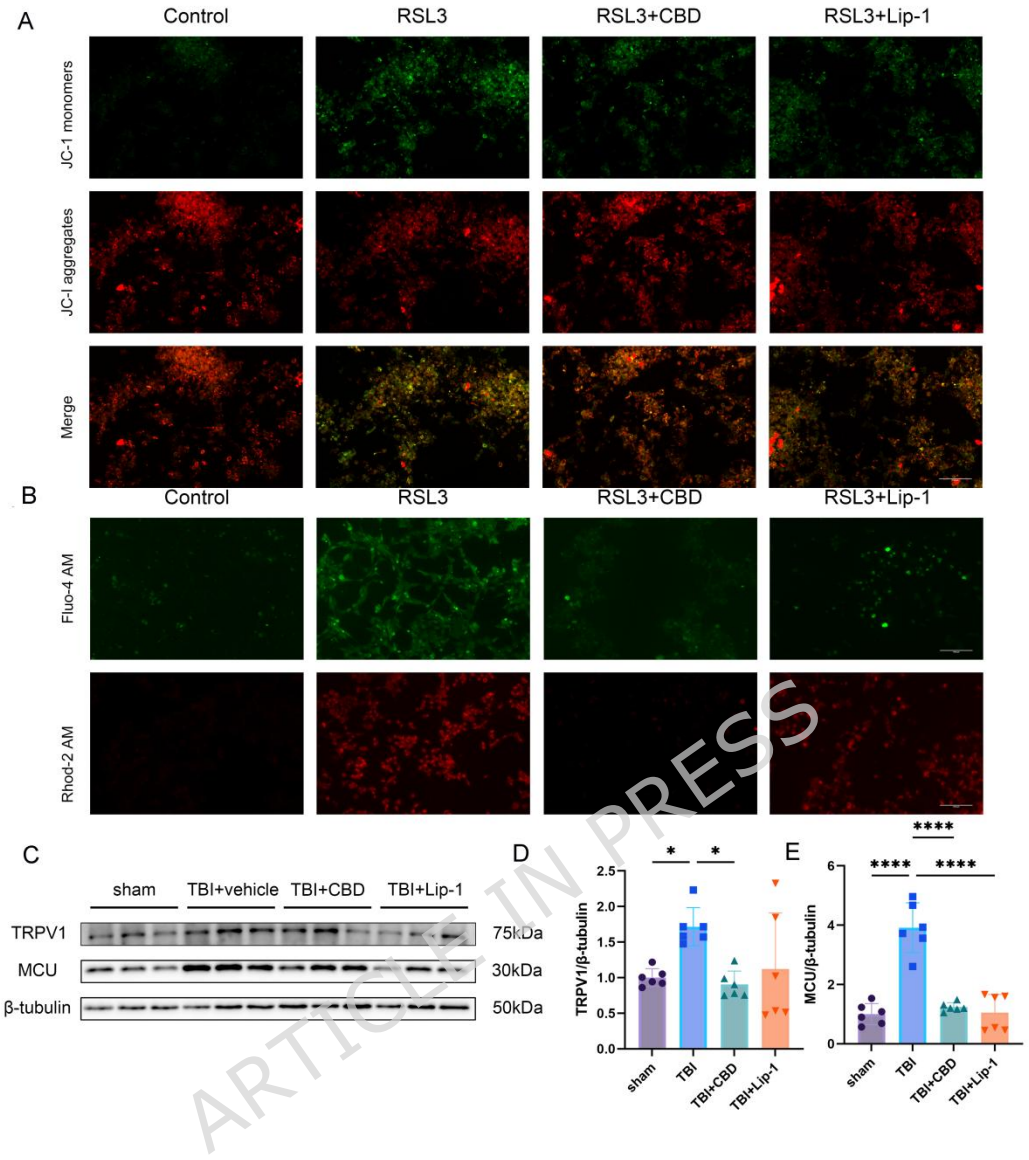

Fig. 5 CBD regulated mitochondrial function and calcium homeostasis in cells. **A** JC-1 staining to evaluate mitochondrial membrane potential. Scale bar = 100 μm. **B** Fluorescence images showing cytosolic and mitochondrial Ca^{2+} levels in HT-22 cells under different treatments. Scale bar=100 μm. **C** Western blotting analysis of TRPV1 and MCU expression in different groups (n = 6). Uncropped Western blotting images were shown in Supplementary Materials. **D** Quantification of TRPV1 and MCU protein

levels, shown as mean ± SD. *$p < 0.05$, ****$p < 0.0001$; ns, not significant.

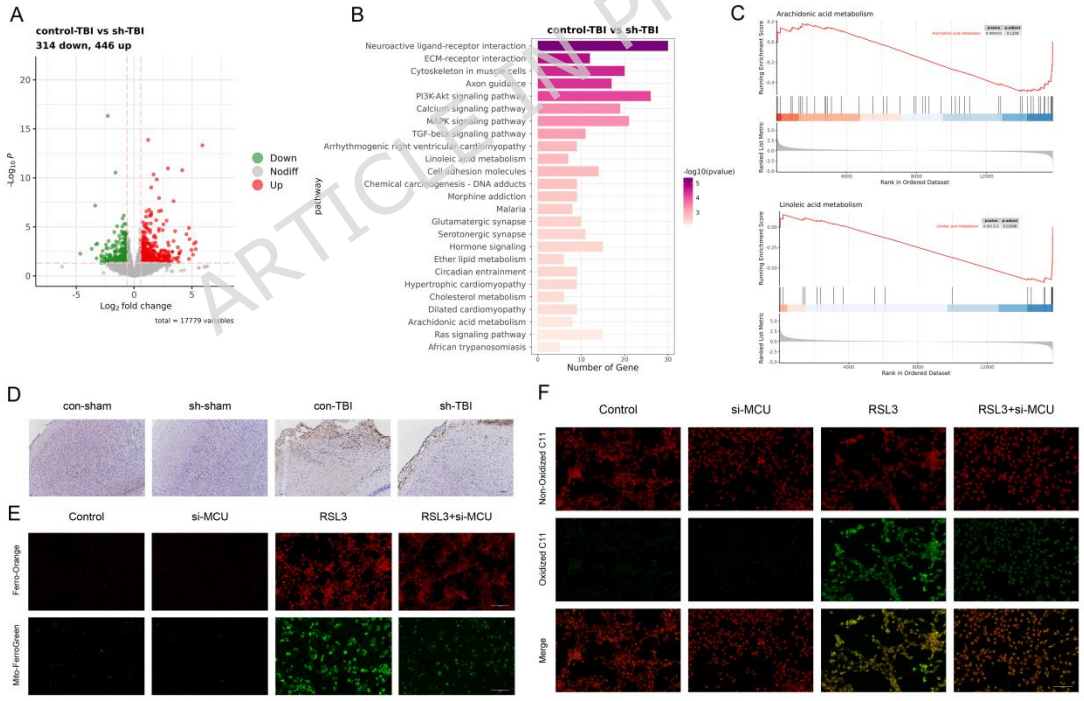

Fig. 6 MCU knockdown reduced iron accumulation and lipid peroxidation after TBI. **A** Distribution of differentially expressed genes between the

control-TBI and sh(MCU)-TBI groups. **B** KEGG enrichment analysis of differentially expressed genes.**C** GSEA analysis of lipid metabolism–related pathways.**D** Perls' Prussian blue staining of brain sections at 1 day post-injury in different groups. Scale bar = 100 μm.**E** Representative images of FerroOrange and Mito-FerroGreen staining in cells. Scale bar = 100 μm. **F** Representative image of BODIPY 581/591 C11 staining for lipid peroxidation. Scale bar = 100 μm.

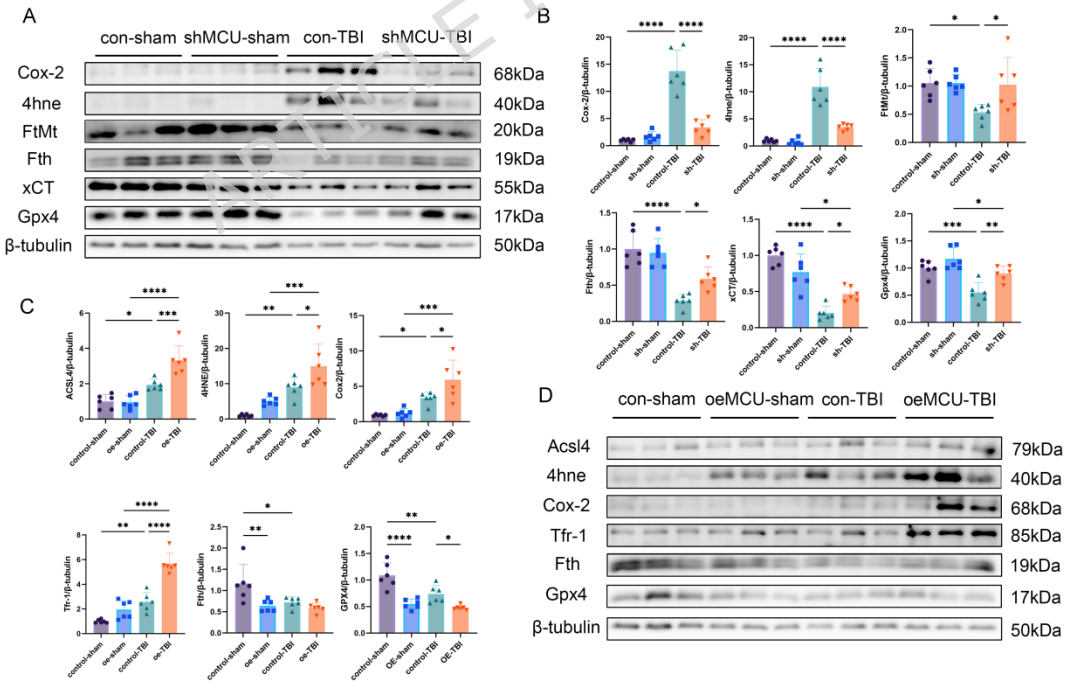

Fig. 7 Effects of MCU knockdown and overexpression on ferroptosis after

TBI. **A** Western blotting analysis of ferroptosis-related proteins after MCU knockdown in different groups (n = 6). Uncropped WB images were shown in Supplementary Materials. **B, C** Quantification of protein expression levels, shown as mean ± SD. *$p < 0.05$, **$p < 0.01$, ***$p < 0.001$, ****$p < 0.0001$; ns, not significant. **D** Western blotting analysis of ferroptosis-related proteins after MCU overexpression in different groups (n = 6). Uncropped Western blotting images were shown in Supplementary Materials.

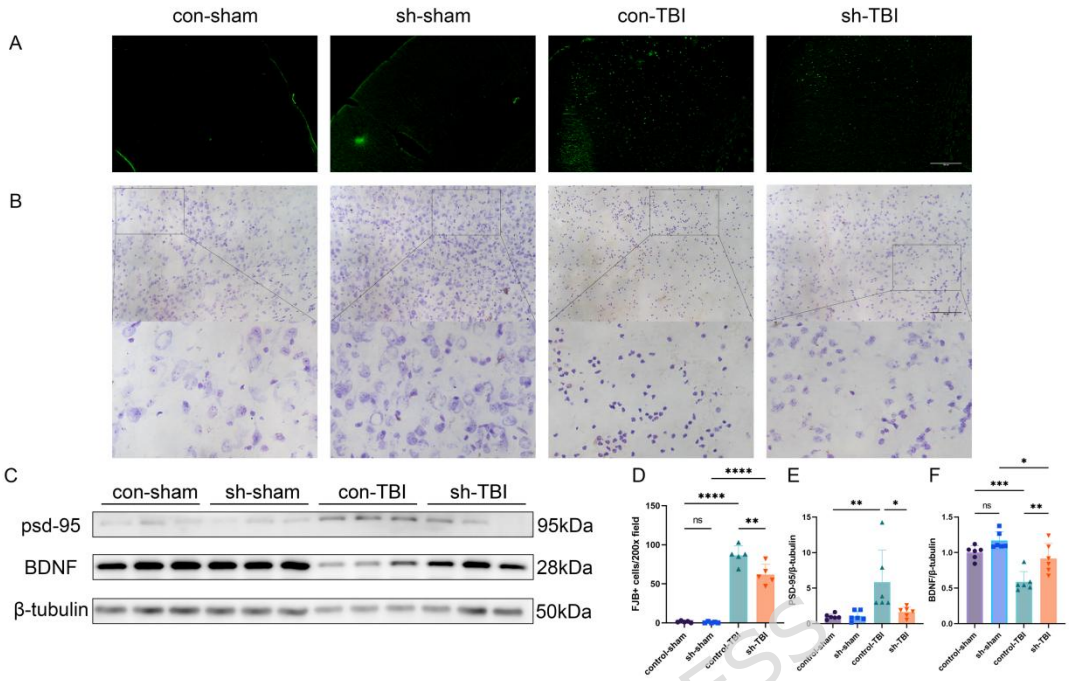

Fig. 8 MCU knockdown alleviated TBI-induced neuronal injury and degeneration. **A** Representative FJB staining images indicating neuronal degeneration. Scale bar = 100 μm.**B** Nissl staining showing neuronal morphological changes in different groups. Scale bar = 100 μm. **C, E, F** Western blotting analysis of psd-95 and BDNF protein levels (n = 6). β-Tubulin served as the internal control. Uncropped Western blotting images were shown in Supplementary Materials. **D** The number of Fth-positive neurons. *$p < 0.05$, **$p < 0.01$,***$p < 0.001$; ns, not significant.

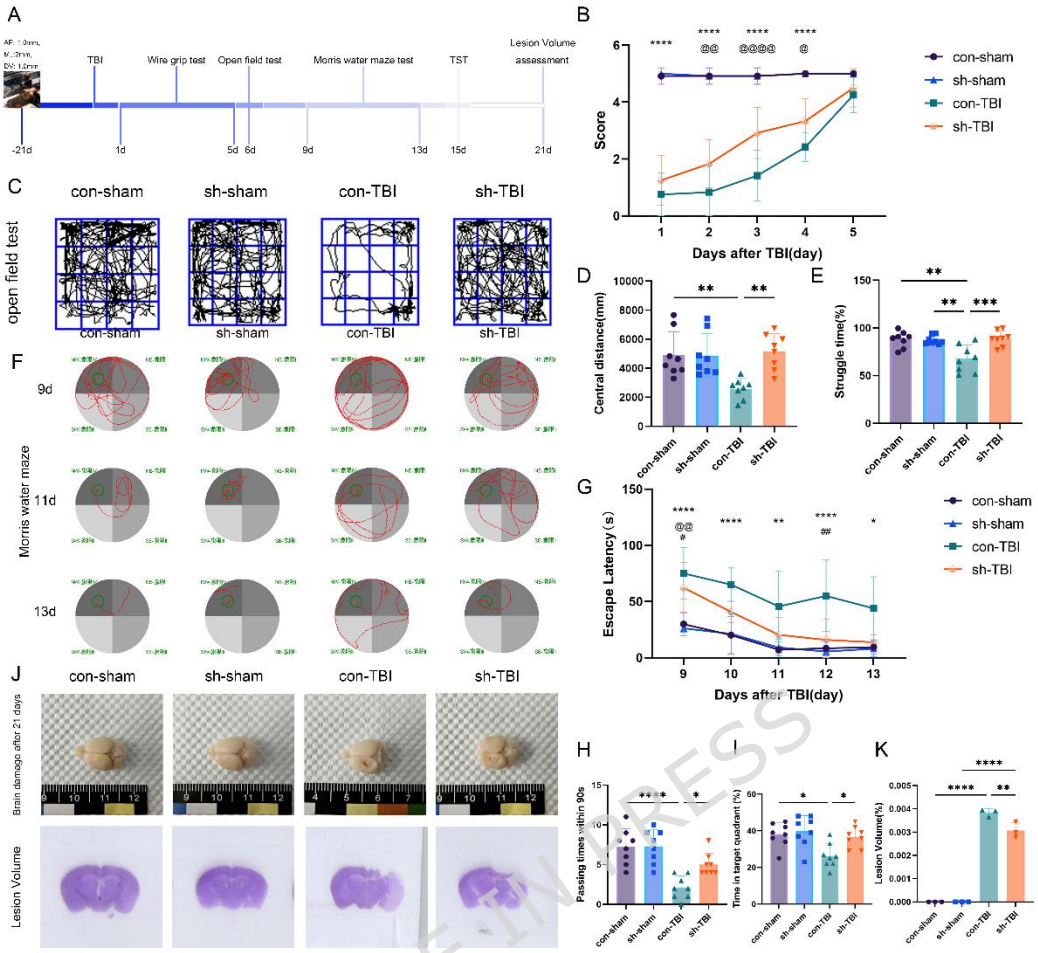

Fig. 9 MCU knockdown improved motor and cognitive performance after TBI. **A** Schematic timeline of behavioral and brain lesion volume analyses. **B** Wire-grip test for motor function (n = 8). **C** Open field test assessing locomotor activity (n = 8).**D** Quantification of central distance traveled in the open field test (n = 8). **E** Immobility time in the tail suspension test (n = 8).**F** Representative images from the Morris water maze test. **G, H, I** Statistical analysis of the Morris water maze test (n = 8). **J** H&E-stained brain sections at 21 days post-injury. **J** Quantification of brain lesion volume at 21 days post-TBI (n = 3). *$p < 0.05$, **$p < 0.01$, ***$p < 0.001$,

****$p < 0.0001$; ns, not significant.

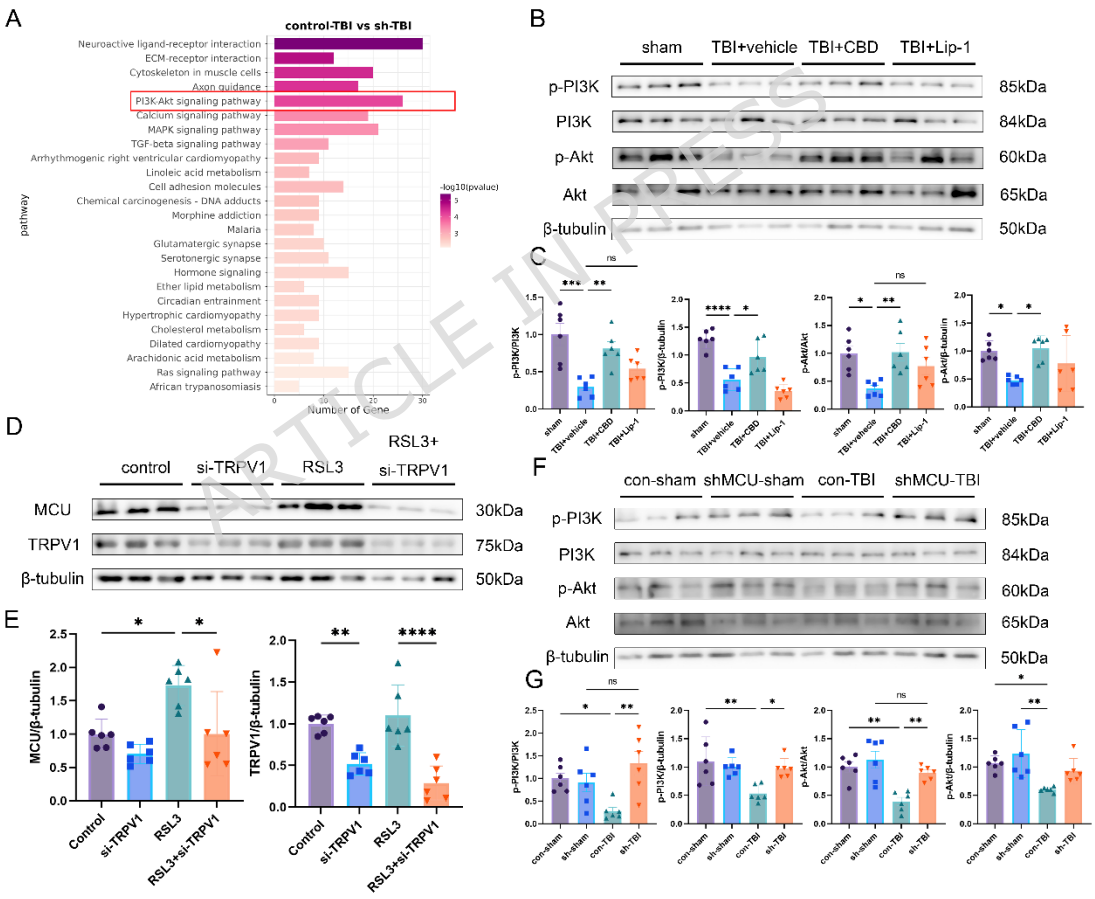

Fig. 10 CBD inhibited ferroptosis signaling pathways activated by TBI. **A** Top 25 significantly enriched KEGG pathways based on DEGs from

transcriptomic analysis. **B, D, F** Western blotting bands of key pathway proteins (n = 6). Uncropped Western blotting images were shown in Supplementary Materials. **C, E, G** Quantification of protein levels, shown as mean ± SD. *$p < 0.05$, **$p < 0.01$, ****$p < 0.0001$; ns, not significant.

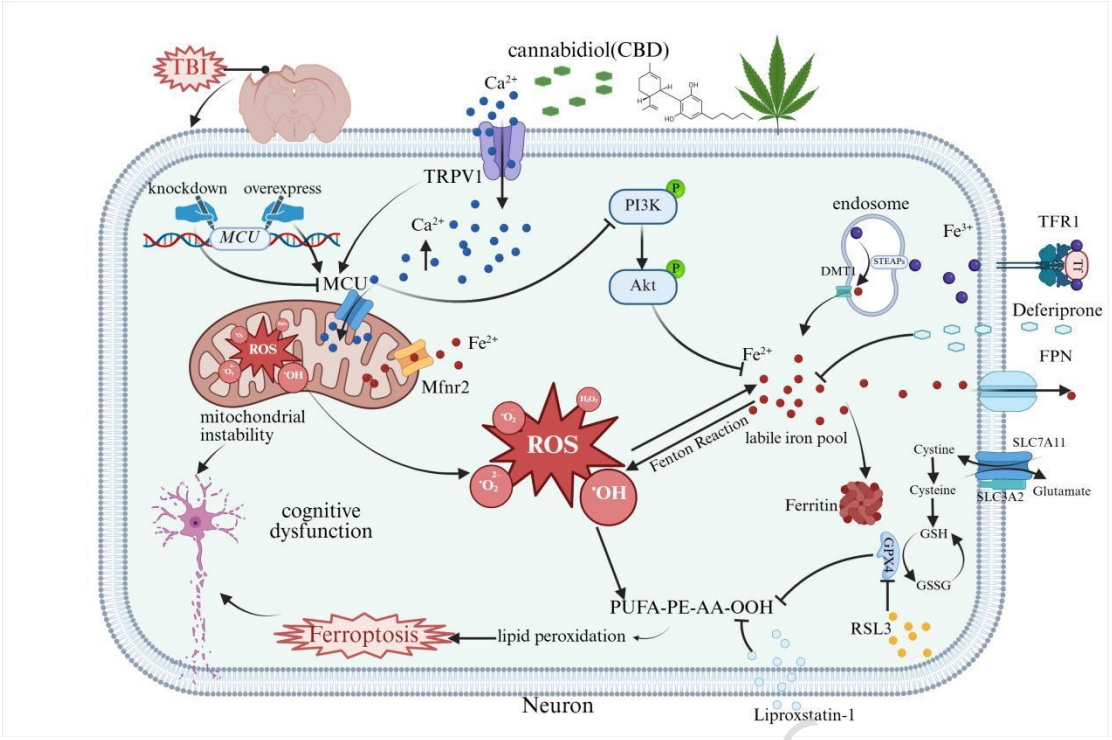

Fig. 11 Summary diagram of research results.